The Astrophysical Journal, 971:31 (20pp), 2024 August 10 https://doi.org/10.3847/1538-4357/ad54b2

Orbits and Dynamical Masses for Six Binary Systems in the Hyades Cluster

Guillermo Torres[1], Gail H. Schaefer[2], Robert P. Stefanik[1], David W. Latham[1], Andrew F. Boden[3], Narsireddy Anugu[2], Jeremy W. Jones[2], Robert Klement[4], Stefan Kraus[5], Cyprien Lanthermann[2], and John D. Monnier[6]
[1] Center for Astrophysics | Harvard & Smithsonian, 60 Garden St., Cambridge, MA 02138, USA; gtorres@cfa.harvard.edu
[2] The CHARA Array of Georgia State University, Mount Wilson Observatory, Mount Wilson, CA 91203, USA
[3] California Institute of Technology, Mail Code 11-17, 1200 East California Boulevard, Pasadena, CA 91125, USA
[4] European Organisation for Astronomical Research in the Southern Hemisphere (ESO), Casilla 19001, Santiago 19, Chile
[5] Astrophysics Group, Department of Physics & Astronomy, University of Exeter, Stocker Road, Exeter, EX4 4QL, UK
[6] Astronomy Department, University of Michigan, Ann Arbor, MI 48109, USA
Received 2024 May 8; revised 2024 May 31; accepted 2024 May 31; published 2024 August 2

Abstract

We report long-baseline interferometric observations with the CHARA Array that resolve six previously known double-lined spectroscopic binary systems in the Hyades cluster, with orbital periods ranging from 3 to 358 days: HD 27483, HD 283882, HD 26874, HD 27149, HD 30676, and HD 28545. We combine those observations with new and existing radial-velocity measurements, to infer the dynamical masses for the components as well as the orbital parallaxes. For most stars, the masses are determined to be better than 1%. Our work significantly increases the number of systems with mass determinations in the cluster. We find that, while current models of stellar evolution for the age and metallicity of the Hyades are able to reproduce the overall shape of the empirical mass–luminosity relation, they overestimate the *V*-band fluxes by about 0.1 mag between 0.5 and 1.4 $M_{\odot}$. The disagreement is smaller in *H*, and near zero in *K*, and depends somewhat on the model. We also make use of the TESS light curves to estimate rotation periods for our targets, and detect numerous flares in one of them (HD 283882), estimating an average flaring rate of 0.44 events per day.

Unified Astronomy Thesaurus concepts: Radial velocity (1332); Binary stars (154); Interferometric binary stars (806); Spectroscopic binary stars (1557); Stellar masses (1614)

Materials only available in the online version of record: machine-readable tables

1. Introduction

Optical interferometry has a long history of making fundamental contributions to many areas of astrophysics (see, e.g., Quirrenbach 2001a, 2001b; Monnier 2003, 2007; Eisenhauer et al. 2023). Classical applications in stellar astronomy include, among many others, the determination of orbits of close binary stars, the measurement of angular diameters and limb darkening properties, and the imaging of stellar surfaces. It was just over a century ago that the first orbit of a binary system (Capella, α Aur, $P = 104$ days) was measured with a 6 m baseline Michelson interferometer on the 100 inch telescope on Mount Wilson (Anderson 1920; Merrill 1922). That orbit is remarkably accurate, even by today's standards. With baselines of an ever increasing length, closer and closer binaries can be resolved, now reaching down to periods of an order of a day for nearby systems. One recent example is HD 284163 (Torres et al. 2024a), with a period of 2.39 days.

A common scientific objective of long-baseline optical and near-infrared interferometry is the determination of dynamical masses for double-lined spectroscopic binaries. The mass of a star is a key ingredient for constraining stellar evolution models, and is most useful when its precision is better than about 3% (see, e.g., Torres et al. 2010). The constraint on models becomes even stronger when the age and metallicity of the system are also known, as is the case for binaries that are members of well-studied clusters. This reduces the number of free parameters in the comparison with theory. The example of HD 284163 mentioned above is a good illustration of this situation. That system is part of a select group of seven double-lined spectroscopic binaries in the Hyades cluster, whose radial velocities (RVs) have been monitored for many years at the Center for Astrophysics (CfA). We have also been targeting this sample recently with the Center for High Angular Resolution Astronomy (CHARA) Array, with the aim of resolving these systems and determining their component masses. In one case, we also make use of archival observations from the Palomar Testbed Interferometer (PTI; Wallace et al. 1998; Colavita et al. 1999).

The present paper reports new, high-precision dynamical mass determinations for the remaining six Hyades binaries in this sample, significantly increasing the list of systems in the Hyades with such measurements. A benefit of astrometric–spectroscopic binaries such as these is that they also yield a model-independent measure of the distance (orbital parallax). We take advantage of this to improve the empirical mass–luminosity relation in the Hyades, at both visual and near-infrared wavelengths.

The plan for the paper is as follows. The selection and properties of our sample are explained in Section 2. The interferometric and spectroscopic observations of the six systems are described in Sections 3 and 4, respectively, and are followed in Section 5 by a general description of our analysis methods that combine both types of observations to infer the masses and orbital parallaxes. Section 6 then presents our results, with separate subsections for each system. In Section 7, we discuss stellar activity and present measurements of the rotation periods by making use of the light curves from

Table 1
Sample of Targets

Target	Gaia R.A. (hh:mm:ss)	Gaia Decl. (dd:mm:ss)	Gaia ID	Period (day)	G (mag)	$\pi_{\rm Gaia}$ (mas)	RUWE	Aliases
HD 27483	04:20:52.838	+13:51:51.74	3310615565476268032	3.06	6.05	21.131 ± 0.032	1.120	vB 34, Han 230, HR 1358
HD 283882	04:49:13.085	+24:48:09.38	147182172683187712	11.9	9.23	20.327 ± 0.033	1.500	vB 117, BD+24 692, V808 Tau
HD 26874	04:15:42.562	+20:49:10.71	49365087086285184	55.1	7.65	20.307 ± 0.044	1.826	vB 162
HD 27149	04:18:01.965	+18:15:24.00	47620265212420096	75.7	7.37	21.606 ± 0.042	1.936	vB 23, Han 178, V1232 Tau
HD 30676	04:50:24.038	+17:12:09.03	3406103958460672768	224.9	6.96	23.923 ± 0.458	19.275	vB 119
HD 28545	04:30:34.988	+15:44:01.97	3312631623125272448	358.5	8.67	17.520 ± 0.399	21.024	vB 182, Han 491, Pels 61

Note. Coordinates, G-band magnitudes, parallaxes, and renormalized unit weight errors (RUWE) are from the Gaia DR3 catalog. The Gaia parallaxes listed are the nominal catalog values, with the addition of zero-point corrections as advocated by Lindegren et al. (2021b). See Section 8 for corrected Gaia parallaxes for HD 30676 and HD 28545 that account for the orbital motion detected by Gaia.

the Transiting Exoplanet Survey Satellite (TESS) mission (Ricker et al. 2015). The mass determinations and absolute magnitudes are compared in Section 8 with other observations in the Hyades, and with current stellar evolution models. We summarize our conclusions in Section 9.

2. Sample

The list of targets for this project was drawn from a spectroscopic survey of stars in the Hyades region, carried out for more than 40 yr at the CfA. That survey has now been essentially completed. We selected double-lined spectroscopic binary systems with orbital periods less than a year, and with the best determined spectroscopic orbits such that the absolute masses could reasonably be expected to be established to better than a few percent, given suitably precise inclination angles from the CHARA Array. The systems were chosen to be bright enough to be accessible with CHARA ($H < 7.5$).

Of the seven FGK targets we initially selected, results for HD 284163 have already been reported separately (Torres et al. 2024a), as mentioned earlier. The other six are listed in Table 1, with their orbital periods as well as coordinates, source identifiers, and parallaxes from the Gaia DR3 catalog (Gaia Collaboration et al. 2023). Other common names sometimes used in the literature are given there as well. We include the Gaia renormalized unit weight error (RUWE), which is an indicator of the quality of the astrometric solution. It is typically close to unity for sources in which a single-star model provides a good description of the astrometric observations (Lindegren 2018). RUWE values greater than about 1.4 can be a sign of unmodeled binary motion (Lindegren et al. 2021a), or other problems with the fit. Interestingly, Table 1 shows a trend of increasing RUWE values with orbital period, consistent with an increase in the amplitude of the astrometric signal one would generally expect.[7]

All of our targets have been shown to be bona fide members of the Hyades cluster (see, e.g., Griffin & Gunn 1981; Tomkin 2003; Griffin 2012).

3. Interferometric Observations

3.1. CHARA Array Observations

The CHARA Array is a long-baseline optical/infrared interferometer located at Mount Wilson Observatory and operated by Georgia State University (ten Brummelaar et al. 2005). The CHARA Array combines the light from six 1 m telescopes with baselines ranging from 34 to 331 m. We observed the sample of Hyades binaries using the MIRC-X combiner in the H band (Anugu et al. 2020) on 10 nights, and MYSTIC in the K band (Setterholm et al. 2023) on the last seven of those nights. MIRC-X and MYSTIC operate simultaneously to combine the light from all six telescopes (S1, S2, E1, E2, W1, and W2), providing spectrally dispersed visibilities on up to 15 baselines and closure phases on up to 20 triangles. Both instruments were used in their low spectral resolution mode (prism $R \sim 50$). A log of the CHARA observations is given in Table 2.

Each observation consisted of recording 10 minutes of fringe data followed by a shutter sequence to measure backgrounds, foregrounds, and the ratio of light between the fringe data and the photometric channels for each telescope. We interspersed observations of single, unresolved calibrator stars between the binary observations to calibrate the interferometric transfer function. The calibrators, adopted angular diameters (Bourgés et al. 2014), and nights on which they were observed are listed in Table 3. The data were reduced using the standard MIRC-X/MYSTIC pipeline[8] (version 1.3.5; Anugu et al. 2020). We used an integration time of 2.5 minutes while reducing the data. The calibrated OIFITS files will be available through the Jean-Marie Mariotti Center (JMMC) Optical Interferometry Database.[9] As part of the reduction process, the calibrators were calibrated against each other and visually inspected; no evidence of binarity was detected in the calibrators.

We used a binary grid search procedure[10] (Schaefer et al. 2016) written in IDL to solve for the separation (ρ), position angle east of north (θ) on the International Celestial Reference System, and the flux ratio (F_2/F_1). The apparent sizes of the stars are unresolved by our observations, even at the longest baselines. Consequently, we adopted fixed stellar angular diameters for the primary and secondary components, and list these in Table 4. They were estimated from preliminary masses for the components, and radii as predicted by stellar evolution models described later. During the fitting process, we divided the wavelengths in the OIFITS files by systematic correction factors of 1.0054 ± 0.0006 for MIRC-X and 1.0067 ± 0.0007 for MYSTIC (J. D. Monnier 2024, private communication). The CHARA measurements for the binary positions are

[7] For unresolved binary systems, Gaia only measures the motion of the photocenter. The amplitude of this motion will depend not only on the period but also on the masses and relative brightness of the components.

[8] https://gitlab.chara.gsu.edu/lebouquj/mircx_pipeline.git

[9] https://www.jmmc.fr/english/tools/data-bases/oidb/

[10] http://www.chara.gsu.edu/analysis-software/binary-grid-search

Table 2
Log for Observations at the CHARA Array

ID	UT Date	Instrument	Science Targets
01	2020 Oct 22	MIRC-X	HD 283882 (5T), HD 27483 (4T, 5T), HD 26874 (5T), HD 27149 (5T)
02	2020 Oct 23	MIRC-X	HD 283882 (6T), HD 27483 (5T), HD 30676 (5T), HD 28545 (5T)
03	2020 Nov 12	MIRC-X	HD 27483 (6T), HD 283882 (5T), HD 26874 (5T), HD 27149 (5T)
04	2021 Oct 6[a]	MIRC-X/MYSTIC	HD 283882 (4T, S1S2W1W2)
05	2021 Oct 22	MIRC-X/MYSTIC	HD 283882 (5T)
06	2021 Nov 19[b]	MIRC-X/MYSTIC	HD 27483 (6T), HD 284163 (6T), HD 26874 (6T)
07	2021 Dec 20	MIRC-X/MYSTIC	HD 26874 (6T), HD 283882 (6T), HD 27149 (6T), HD 28545 (5T), HD 30676 (5T)
08	2022 Oct 25	MIRC-X/MYSTIC	HD 27149 (5T), HD 30676 (5T), HD 26874 (5T), HD 27483 (5T), HD 28545 (5T), HD 27483 (5T)
09	2022 Nov 15[c]	MIRC-X/MYSTIC	HD 30676 (4T, 3T), HD 27149 (4T, 3T), HD 27483 (4T), HD 28545 (4T), HD 26874 (3T), HD 283882 (3T)
10	2023 Feb 17	MIRC-X/MYSTIC	HD 30676 (5T)

Notes. The E1-W2-W1-S2-S1-E2 configuration was used on each night with MIRC-X in H-Prism50 mode and MYSTIC in K-Prism49 mode. Targets that were observed with all six telescopes are marked with "6T" in parentheses. After losing delay on the E1 cart in the western part of the sky, we continued observing targets with five telescopes ("5T").
[a] On UT 2021 October 6, MYSTIC was not cophased properly with MIRC-X, so only the W1-W2 and S2-S1 fringes were recorded on MYSTIC for HD 283882. No binary fit was done for this target.
[b] On UT 2021 November 19, data on HD 27483 were recorded at a gain of 1 on MYSTIC. No binary fit was done for the MYSTIC data on this target.
[c] On UT 2022 November 15, the S1 and S2 telescopes were offline because of a problem with the metrology signal on the S1 delay line cart and a mechanical problem with the drive bearings on the S2 telescope.

Table 3
Adopted Calibrator Angular Diameters for the Observations at the CHARA Array

Calibrator	UDH (mas)	UDK (mas)	σ_{UD} (mas)	Nights Observed
HD 17660	0.3053	0.3069	0.0073	1, 2, 3
HD 20150	0.3499	0.3506	0.0127	9
HD 23288	0.2277	0.2282	0.0068	9
HD 24442	0.3533	0.3547	0.0084	5, 7
HD 24702	0.2441	0.2450	0.0057	5, 6
HD 27561	0.3037	0.3047	0.0076	8
HD 27627	0.2727	0.2740	0.0062	1, 2, 3, 8, 9
HD 27808	0.2748	0.2758	0.0066	1, 2, 3, 4, 5, 6, 7, 9
HD 27819	0.4312	0.4321	0.0400	10
HD 28406	0.2766	0.2775	0.0069	1, 2, 3, 6, 7, 8, 9
HD 36667	0.2839	0.2849	0.0069	5, 6, 8, 9

Note. Uniform-disk diameters adopted for the calibrators in the *H* band (UDH) and *K* band (UDK) from the JMMC Catalog of stellar diameters (Bourgés et al. 2014). The nights observed correspond to the ID column in Table 2. During the observations of HD 24442 on UT 2021 October 22 and HD 24702 on UT 2021 November 19, the visibilities on the S1 baselines suffered from bad calibration caused by vibrations induced by the cable puller when the S1 delay line cart moved backwards while the star was at low elevations in the east; the S1 baselines were flagged as bad in these data files. HD 27819 was observed as a brighter calibrator on UT 2023 February 17. Although there are conflicting reports in the literature about whether it is a binary (see discussion by Morales et al. 2022), HD 27819 was used as an interferometric calibrator (Boyajian et al. 2009; Baines et al. 2018) and has a limb-darkened diameter of 0.489 ± 0.007 mas measured by Salsi et al. (2021). The closure phases show variations less than $\pm 3°$, but the MIRC-X and MYSTIC data do not give consistent results when fitting for a binary companion.

reported in Table 5. As is customary, the 1σ uncertainties in the positions are defined by the major and minor axes of the error ellipse for each observation (σ_{maj}, σ_{min}). The orientation of the error ellipse, given by the position angle ψ, is dependent on the *uv* coverage during the observation.

Table 4
Adopted Angular Diameters for Primary and Secondary Stars in the Hyades Binaries

Binary	UD_1 (mas)	UD_2 (mas)
HD 27483	0.265	0.257
HD 283882	0.134	0.127
HD 26874	0.186	0.163
HD 27149	0.199	0.179
HD 30676	0.156	0.126
HD 28545	0.159	0.118

3.2. PTI Observations

Additional, near-infrared, long-baseline interferometric measurements of one of our targets, HD 27149, were conducted with PTI, which was a 110 m baseline *H*- and *K*-band ($\lambda \sim 1.6$ and $\sim 2.2\ \mu$m) interferometer located at Palomar Observatory, and decommissioned in 2008. The PTI is described in full detail elsewhere (Colavita et al. 1999). The instrument gave a minimum fringe spacing of about 4 mas, making the binary orbit of the target readily resolvable.

The PTI interferometric observable used for these measurements is the fringe contrast or "visibility" (specifically, the power-normalized visibility modulus squared, V^2) of the observed brightness distribution on the sky. The measurements we obtained were made in the *K* band, and are given in Table 6. HD 27149 was typically observed in conjunction with two calibration objects, and each observation (or scan) was approximately 130 s long. As in previous publications, PTI V^2 data reduction and calibration follow standard procedures described by Colavita et al. (2003) and Boden et al. (1998), respectively. For this analysis, we used HD 27397 and HD 27459 as our calibration sources, with adopted uniform-disk angular diameters of 0.40 ± 0.07 and 0.38 ± 0.06 mas, respectively. At these diameter estimates, the PTI baselines do not significantly resolve these sources.

Table 5
CHARA Measurements for Our Targets

Target	UT Date	HJD–2,400,000	ρ (mas)	θ (deg)	σ_{maj} (mas)	σ_{min} (mas)	ψ (deg)	F_2/F_1	Instrument
HD 27483	2020 Oct 22	59144.949	1.1649	27.30	0.0014	0.0012	174.72	0.929	MIRC-X
HD 27483	2020 Oct 22	59144.966	1.1548	29.06	0.0016	0.0012	167.48	0.928	MIRC-X
HD 27483	2020 Oct 23	59145.976	1.1069	163.43	0.0067	0.0024	59.20	0.928	MIRC-X
HD 27483	2020 Nov 12	59165.802	1.0672	337.60	0.0013	0.0004	118.77	0.933	MIRC-X
HD 27483	2021 Nov 19	59537.768	1.1955	184.25	0.0080	0.0072	101.50	0.943	MIRC-X

Note. The columns σ_{maj} and σ_{min} represent the major and minor axes of the 1σ error ellipse for each measurement, and ψ gives the orientation of the major axis relative to the direction to the north. All position angles are referred to the International Celestial Reference Frame (effectively J2000). Formal uncertainties for the flux ratios F_2/F_1 in the H or K bands are not reported, as they are typically unrealistically small. A more representative value for the uncertainty is given by the scatter of the measurements from different epochs (see Section 8).

(This table is available in its entirety in machine-readable form in the online article.)

Table 6
PTI K-band Squared Visibility Measurements for HD 27149

UT Date	HJD–2,400,000	$\langle\lambda\rangle$ (μm)	V^2	σ_{V^2}	u (m)	v (m)
2000Sep13	51801.0255	2.2306	0.809	0.074	−36.4936	−98.9544
2000Sep13	51801.0331	2.2266	0.828	0.067	−33.5676	−99.4827
2000Sep13	51801.0402	2.2402	1.028	0.167	−30.7831	−99.9330
2000Oct01	51818.9080	2.2320	0.586	0.570	−58.1778	−92.4689
2000Oct01	51818.9100	2.2290	0.771	0.305	−57.6839	−92.6953

Note. $\langle\lambda\rangle$ is the flux-weighted center-band wavelength. The last two columns represent the projected baselines.

(This table is available in its entirety in machine-readable form in the online article.)

4. Spectroscopic Observations

Our sample of objects in Table 1 has been observed spectroscopically at the CfA for a decade or more, as part of a larger program to monitor the RVs of several hundred stars in the Hyades region. The vast majority of the observations for this paper were gathered with two nearly identical echelle instruments (digital speedometers; Latham 1992), which operated until 2010. One was attached to the 1.5 m Wyeth reflector at the (now closed) Oak Ridge Observatory, in the town of Harvard (MA, USA), and the other was attached to the 1.5 m Tillinghast reflector at the Fred L. Whipple Observatory (Mount Hopkins, AZ, USA). These instruments were equipped with intensified photon-counting Reticon detectors that recorded a single echelle order 45 Å wide, centered on the Mg I b triplet near 5187 Å. The resolving power was $R \approx 35{,}000$, corresponding to 8.5 km s^{-1}.

A few observations for one of our targets (HD 28545) were gathered more recently with the Tillinghast Reflector Echelle Spectrograph (TRES; Szentgyorgyi & Fűrész 2007; Fűrész 2008), a bench-mounted, fiber-fed instrument on the 1.5 m telescope in AZ. The TRES CCD detector records 51 orders over the 3800–9100 Å range, at a resolving power of $R \approx 44{,}000$ (6.8 km s^{-1}).

For the digital speedometers, the zero-point of the RVs was monitored by taking sky exposures in the evening and the morning, which were used to calculate and apply small run-to-run corrections to the raw velocities in order to place them on a common system (see Latham 1992). These corrections were typically under 2 km s^{-1}. This native CfA system is slightly offset from the IAU reference frame by 0.14 km s^{-1} (Stefanik et al. 1999), as determined from observations of minor planets in the solar system. In order to remove this shift, we adjusted the velocities by adding +0.14 km s^{-1}. For TRES, changes in the velocity zero-point were monitored with observations of several IAU standard stars, and asteroid observations were then employed to transfer the raw velocities to an absolute system, as with the digital speedometers.

The spectra of all our targets are double lined. RVs were measured using TODCOR, which is a two-dimensional cross-correlation algorithm (Zucker & Mazeh 1994). Templates were selected from a large library of synthetic spectra based on model atmospheres by R. L. Kurucz, and a line list manually tuned to better match real stars (see Nordström et al. 1994; Latham et al. 2002). These templates cover the region centered on the Mg I b triplet, which captures most of the velocity information. The surface gravity for the templates was held at $\log g = 4.5$, which is appropriate for our objects, and we assumed solar metallicity, which is sufficiently close to the Hyades composition for our purposes ([Fe/H] = +0.18; Dutra-Ferreira et al. 2016). To determine the optimal effective temperature and line broadening for each binary component ($T_{\rm eff}$ and $v \sin i$), we ran grids of cross-correlations over broad ranges in those parameters, as described by Torres et al. (2002). We then selected the templates producing the highest correlation coefficient averaged over all exposures. The adopted template parameters are reported in Section 6. We note that, while rotation may be the dominant line broadening mechanism for these stars, what we refer to here as $v \sin i$, for short, includes all other broadening mechanisms, such as macroturbulence (beyond the value of $\zeta_{\rm RT} = 1$ km s^{-1} already built into our templates).

Table 7
CfA Radial Velocities for Our Targets

Target Name	HJD–2,400,000	RV_1 (km s^{-1})	σ_1 (km s^{-1})	RV_2 (km s^{-1})	σ_2 (km s^{-1})
HD 27483	44560.8138	86.21	0.62	−10.82	0.52
HD 27483	44591.7209	41.95	0.54	33.64	0.45
HD 27483	44627.6614	111.22	1.11	−34.88	0.93
HD 27483	44629.6680	−6.49	0.72	83.74	0.60
HD 27483	44887.8474	107.26	0.74	−34.08	0.62

Note. The velocities in this table include all adjustments described in the text.
(This table is available in its entirety in machine-readable form in the online article.)

Experience has shown that the limited number of lines in the narrow wavelength range of the digital speedometers can sometimes introduce subtle biases in the RVs. These errors are caused by spectral lines of the binary components shifting in and out of the spectral window in opposite directions, depending on both the orbital phase and the projected velocity of the Earth relative to the solar system barycenter. We evaluated and corrected for these effects in each of our systems through numerical simulations. We refer the reader to Latham et al. (1996) and Torres et al. (1997a) for further details of that procedure. The measured RVs and formal uncertainties for all our targets are presented together in Table 7. The use of TODCOR allows us to extract for each binary an estimate of the spectroscopic flux ratio between the components (see Zucker & Mazeh 1994), at the mean wavelength of our observations (∼5187 Å). We report these values in Section 6, and use them later to infer the individual brightness of each component.

In addition to our own velocities, the analyses described in the next section made use of RV observations from other sources that extend our time baseline or supplement the phase coverage, and are of sufficient quality to make them useful. These included measurements from the extensive Hyades program conducted by Roger Griffin (Griffin & Gunn 1978, 1981; Griffin 2012), as well as velocities with the CORAVEL spectrometer as reported by Mermilliod et al. (2009). In several cases, we also used velocity measurements taken from the public archive of observations gathered with the Elodie spectrograph,[11] which are typically of high precision. Other RV sources are described below.

5. Orbital Analysis

The CHARA observations and RV measurements for each system were used together to solve for the astrometric and spectroscopic orbital elements simultaneously. The usual spectroscopic elements are the period (P), center-of-mass velocity (γ), primary and secondary velocity semiamplitudes (K_1, K_2), the eccentricity (e) and argument of periastron for the primary (ω_1), expressed for this work as $\sqrt{e}\cos\omega_1$ and $\sqrt{e}\sin\omega_1$, and a reference time of periastron passage ($T_{\rm peri}$). The purely astrometric elements are the angular semimajor axis (a''), the cosine of the orbital inclination angle relative to the line of sight ($\cos i$), and the position angle of the ascending node for J2000.0 (Ω). In order to account for the possibility of systematic shifts in the velocities from outside sources relative to our own, we typically also solved for separate RV offsets (Δ) for each of those sources, along with the other free parameters of our model. These offsets should be added to the corresponding velocities in order to place them on the reference frame of the CfA velocities. For the PTI observations of HD 27149, we included the K-band flux ratio as an additional free parameter.

Our solutions were performed within a Markov Chain Monte Carlo (MCMC) framework, using the EMCEE[12] package of Foreman-Mackey et al. (2013). We applied uniform priors over suitable ranges for all of the above adjustable parameters. Convergence was verified by a visual inspection of the chains. We also required a Gelman–Rubin statistic of 1.05 or smaller (Gelman & Rubin 1992).

As internal measurement errors are not always accurate, but are important for the proper weighting of the various data sets relative to one another, we included additional free parameters in our analysis to represent multiplicative error scaling factors, f, for all uncertainties. We did this for each RV data set, separately for the primary and secondary components, as well as for the CHARA observations and the PTI squared visibilities. These factors were solved for simultaneously and self-consistently with the other free parameters (see Gregory 2005), using log-normal priors.

6. Results

The subsections that follow present a summary of the available spectroscopic data, and the particulars of the orbital analysis for each of our six Hyades binaries, in order of increasing orbital period, as in Table 1. Aside from the component masses, the astrometric–spectroscopic solutions yield the orbital parallax, which we use later to compute the absolute brightness of the components.

6.1. HD 2748

This Hyades object has been known to be a spectroscopic binary for more than eight decades (Christie & Wilson 1938; Young 1939). The first double-lined orbital solution, with a period of 3.06 days, was reported by Northcott & Wright (1952), on the basis of 67 photographic RV measurements made between 1933 and 1951 at the Dominion Astrophysical Observatory. Additional velocities with the CORAVEL instrument have been reported by Mayor & Mazeh (1987) and Mermilliod et al. (2009), the latter ones largely superseding the former ones, after a zero-point adjustment and changes to the uncertainties. As described in more detail by Griffin (2012), these two recent data sets are not exactly the same, and the earlier publication has the identities of the primary and secondary reversed. Confusingly, the 2009 paper has the wrong assignments in several instances. Mayor & Mazeh (1987) reported RVs at five epochs that are not included in the Mermilliod et al. (2009) set. Based on a comparison of the observations in common, we have scaled the original uncertainties of those five measurements by a factor 1.6, and shifted them to the Mermilliod et al. (2009) system by applying the same average adjustment of +0.34 km s^{-1} used by those authors. Altogether, there are 20 CORAVEL observations of the primary and 19 of the secondary taken between 1979 and 1993, excluding two that were gathered at times when the lines

[11] http://atlas.obs-hp.fr/elodie/

[12] https://emcee.readthedocs.io/en/stable/index.html

of the two stars were severely blended. We have also used 25 pairs of velocities (1986–2010) by Griffin (2012), with the relative weights assigned by that author, and adopting his error of 0.70 km s^{-1} for an observation of unit weight. Compared to these more recent measurements, the ones by Northcott & Wright (1952) are so much poorer that they provide no benefit for our analysis, not even for improving the period. Consequently, we have not used them.

Our own spectroscopic contribution consists of 114 observations made with the digital speedometers between 1980 and 2001, with signal-to-noise ratios (S/Ns) ranging from 11 to 81 per resolution element. The synthetic templates adopted for the cross-correlations with TODCOR have temperatures of 6500 K for both components, and rotational broadenings of 20 and 12 km s^{-1} for the primary and secondary. The velocities have been listed earlier in Table 7. We determined a spectroscopic flux ratio between the components of $(F_2/F_1)_{sp} = 0.854 \pm 0.027$, at the mean wavelength of our observations.

HD 27483 was also observed with PTI by Konacki & Lane (2004), who presented a spectroscopic–astrometric orbital solution based on the RV measurements of Mayor & Mazeh (1987). However, as the authors reported, the binary was only partially resolved, causing a strong degeneracy between the semimajor axis and the brightness ratio. This compelled them to assume an arbitrary brightness ratio of unity. Their mass determinations have formal uncertainties approaching 10%. We experimented with incorporating those PTI visibilities into our analysis, but found no improvement in any of the elements compared to using only the CHARA observations. Consequently, those PTI observations have not been used here.

In addition to the standard orbital elements and error inflation factors for each data set described earlier, we allowed for systematic offsets (Δ_G, Δ_M) for the Griffin (2012) and Mermilliod et al. (2009) velocities relative to ours. Initial spectroscopic-only solutions indicated a negligible eccentricity, and in such cases, the time of periastron passage is poorly determined. To avoid this indeterminacy in our analysis, instead of T_{peri}, we solved for the time of nodal passage T_{node}, which is always well determined. It corresponds to the time of maximum primary velocity. Table 8 presents the results, along with other derived properties including the masses. The eccentricity is not statistically significant, and we infer a 3σ upper limit of $e = 0.002$. The astrometric orbit with our CHARA measurements is shown in Figure 1, and the RVs can be seen in Figure 2.

HD 27483 has a distant white dwarf companion, first detected spectroscopically by Böhm-Vitense (1993) from excess flux in an IUE spectrum. The Gaia DR3 catalog has no entry for this companion. It was spatially resolved using the Hubble Space Telescope (HST) by Barstow et al. (2001), who found it to be about 1.″3 due north, and 1.96 mag fainter in the UV. Additional measurements of the relative position and brightness with HST and ground-based adaptive optics were reported by Zhang et al. (2023). These authors combined those constraints with the astrometric acceleration of the primary from the proper-motion difference between Gaia and Hipparcos, to infer a mass for the white dwarf of $0.798^{+0.10}_{-0.04}\ M_\odot$, an orbital period of 184^{+65}_{-30} yr, and an orbital inclination of $30^{+13\circ}_{-15}$. The system is therefore triple. This is not unexpected, as Tokovinin et al. (2006) have shown that more than 95% of spectroscopic binaries with periods under about 3 days have additional components. Zhang et al. (2023) noted that the orbit of the white dwarf appears reasonably well aligned with that of the inner binary. They based this conclusion on an adopted inclination angle for the inner binary of $45.^\circ1 \pm 1.^\circ7$ from Konacki & Lane (2004), which is similar to ours.

Table 8
Results of Our Orbital Analysis for HD 27483

Parameter	Value
P (day)	$3.05911946^{+0.00000041}_{-0.00000041}$
T_{node} (HJD−2,400,000)	$49207.19931^{+0.00053}_{-0.00053}$
a'' (mas)	$1.2152^{+0.0021}_{-0.0021}$
$\sqrt{e}\cos\omega_1$	$+0.005^{+0.017}_{-0.018}$
$\sqrt{e}\sin\omega_1$	$-0.019^{+0.021}_{-0.013}$
$\cos i$	$0.7042^{+0.0017}_{-0.0017}$
Ω (deg)	$10.44^{+0.16}_{-0.16}$
γ (km s^{-1})	$+38.086^{+0.049}_{-0.049}$
K_1 (km s^{-1})	$71.642^{+0.086}_{-0.086}$
K_2 (km s^{-1})	$73.273^{+0.070}_{-0.070}$
Δ_G (km s^{-1})	$-0.27^{+0.14}_{-0.14}$
Δ_M (km s^{-1})	$-1.29^{+0.23}_{-0.23}$
f_{CHARA}	$2.94^{+0.62}_{-0.41}$
$f_{CfA,1}$ and σ_1 (km s^{-1})	$0.886^{+0.065}_{-0.055}$, 0.80
$f_{CfA,2}$ and σ_2 (km s^{-1})	$0.867^{+0.062}_{-0.053}$, 0.66
$f_{G,1}$ and σ_1 (km s^{-1})	$1.19^{+0.22}_{-0.14}$, 0.99
$f_{G,2}$ and σ_2 (km s^{-1})	$0.97^{+0.18}_{-0.12}$, 0.80
$f_{M,1}$ and σ_1 (km s^{-1})	$1.63^{+0.32}_{-0.21}$, 1.79
$f_{M,2}$ and σ_2 (km s^{-1})	$1.14^{+0.24}_{-0.16}$, 1.10
Derived quantities	
e	$0.00062^{+0.00072}_{-0.00041}$
ω_1 (deg)	280^{+36}_{-128}
i (deg)	$45.24^{+0.13}_{-0.13}$
$M_1 (M_\odot)$	$1.363^{+0.010}_{-0.010}$
$M_2\ (M_\odot)$	$1.3323^{+0.0099}_{-0.0099}$
$q \equiv M_2/M_1$	$0.9777^{+0.0015}_{-0.0015}$
$a\ (R_\odot)$	$12.341^{+0.030}_{-0.030}$
π_{orb} (mas)	$21.174^{+0.072}_{-0.073}$
Distance (pc)	$47.23^{+0.16}_{-0.16}$
T_{peri} (HJD−2,400,000)	$49209.58^{+0.31}_{-1.09}$

Note. $f_{CfA,1}$ and $f_{CfA,2}$ are the scale factors for the internal errors of the CfA RV velocities of the primary and secondary. A similar notation is used for the RVs of Griffin (2012) and Mermilliod et al. (2009). Values following these scale factors on the same line are the weighted rms residuals, after application of the scale factors.

6.2. HD 283882

Double lines in the spectra of HD 283882 were first mentioned by Wilson (1948), and later also by Young (1974), who provided the first five RV measures of each component made in 1971. Griffin & Gunn (1978) observed it more extensively, and derived a spectroscopic orbit with a period of 11.9 days. That set of observations was augmented (and the date of the last one corrected) by Griffin (2012), giving a much more complete phase coverage in the rather eccentric orbit. After rejecting several observations at strongly blended phases, and a few others that Griffin (2012) also considered unreliable, there are 60 measurements of the primary and 62 of the secondary made between 1973 and 2010, which we used for our analysis below. We adopted the relative weighting

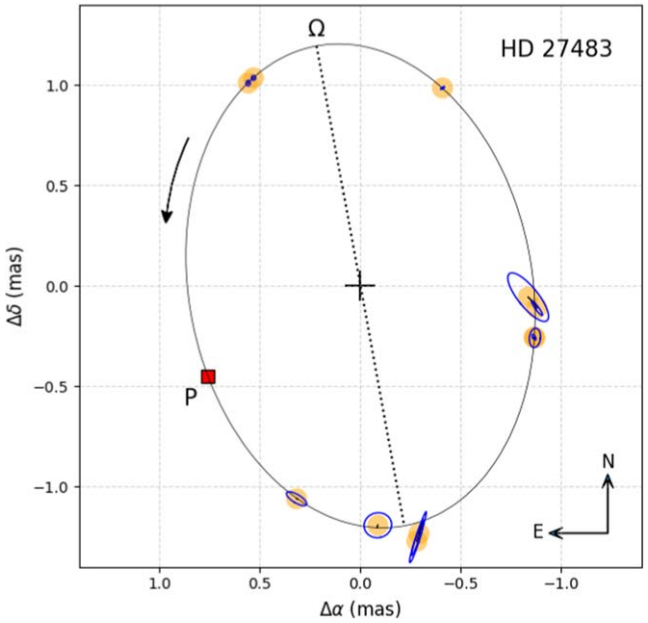

Figure 1. Astrometric measurements for HD 27483, with our model for the orbit. Each observation is highlighted with an orange circle for clarity, and is shown with its error ellipse. Short line segments connect the measured positions with the predicted ones from our model. The line of nodes is represented with a dotted line, and the ascending node is indicated with the "Ω" symbol. Periastron is marked with the red square labeled "P."

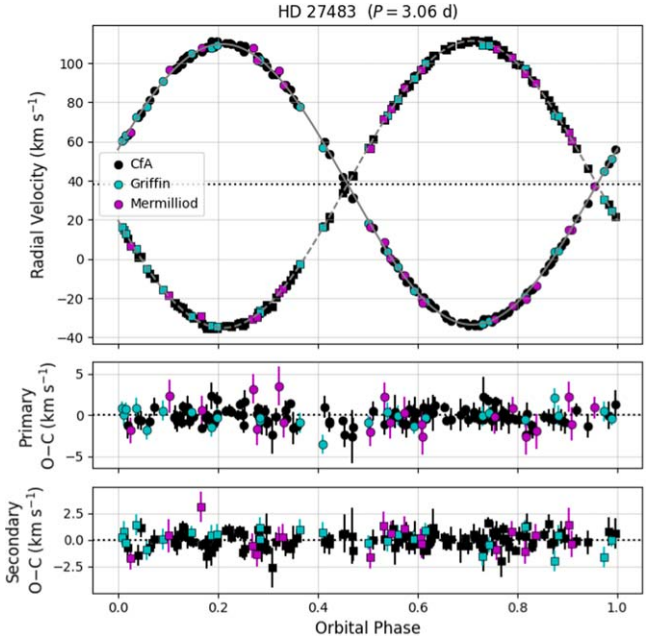

Figure 2. RV measurements for HD 27483 from the CfA and other literature sources, along with our adopted model for the spectroscopic orbit. Phase zero corresponds to the formal time of periastron passage listed in Table 8. The dotted line represents the center-of-mass velocity. Residuals with the corresponding error bars are shown in the lower panels. Some error bars are smaller than the symbol size.

recommended by Griffin, along with his stated uncertainty of 0.55 km s^{-1} for an observation of unit weight.

A total of 40 observations for HD 283882 were collected at the CfA with the digital speedometers between 1985 and 1995, of which one giving abnormally large velocity residuals for both components was rejected. S/Ns are relatively low in this case, and range between 8 and 17 per resolution element. The cross-correlation templates that were found to give the best results have temperatures of 5000 and 4750 K for the primary and secondary, and rotational broadenings of 6 km s^{-1} for both stars. We estimate the spectroscopic flux ratio between the components to be $(F_2/F_1)_{sp} = 0.524 \pm 0.045$.

There are two other smaller sets of velocities available that were also used in our modeling of HD 283882. One consists of eight primary and six secondary velocities by Mermilliod et al. (2009), made with the CORAVEL instrument (1978–1981), with their corresponding formal uncertainties. The other is a set of six archival velocity measurements for both stars from 2003–2005, which we retrieved from the public Elodie archive. For these, we adopted arbitrary initial uncertainties of 0.5 km s^{-1}, later adjusted by iterations in the analysis below. Even though the five pairs of old measurements by Young (1974) are quite consistent with the orbit model presented in this section, we chose not to incorporate them because of their larger scatter.

The joint solution with the velocities and our CHARA observations is presented in Table 9, and includes additional free parameters to account for possible systematic offsets

Table 9
Results of Our Orbital Analysis for HD 283882

Parameter	Value
P (day)	$11.928690^{+0.0000058}_{-0.0000057}$
T_{peri} (HJD−2,400,000)	$47820.9470^{+0.0022}_{-0.0022}$
a'' (mas)	$2.4144^{+0.0076}_{-0.0077}$
$\sqrt{e}\cos\omega_1$	$+0.0098^{+0.0013}_{-0.0015}$
$\sqrt{e}\sin\omega_1$	$+0.71937^{+0.00054}_{-0.00057}$
$\cos i$	$0.1947^{+0.0018}_{-0.0018}$
Ω (deg)	$353.09^{+0.21}_{-0.21}$
γ (km s^{-1})	$+40.099^{+0.092}_{-0.091}$
K_1 (km s^{-1})	$60.856^{+0.086}_{-0.078}$
K_2 (km s^{-1})	$64.25^{+0.11}_{-0.10}$
Δ_G (km s^{-1})	$-0.75^{+0.11}_{-0.11}$
Δ_M (km s^{-1})	$+0.22^{+0.39}_{-0.36}$
Δ_E (km s^{-1})	$+0.01^{+0.11}_{-0.11}$
f_{CHARA}	$3.26^{+0.78}_{-0.51}$
$f_{CfA,1}$ and σ_1 (km s^{-1})	$1.08^{+0.15}_{-0.11}$, 0.64
$f_{CfA,2}$ and σ_2 (km s^{-1})	$0.961^{+0.127}_{-0.092}$, 1.16
$f_{G,1}$ and σ_1 (km s^{-1})	$1.006^{+0.111}_{-0.086}$, 0.60
$f_{G,2}$ and σ_2 (km s^{-1})	$1.070^{+0.114}_{-0.089}$, 0.79
$f_{M,1}$ and σ_1 (km s^{-1})	$2.92^{+1.06}_{-0.57}$, 1.80
$f_{M,2}$ and σ_2 (km s^{-1})	$1.33^{+0.65}_{-0.30}$, 0.92
$f_{E,1}$ and σ_1 (km s^{-1})	$0.234^{+0.166}_{-0.074}$, 0.104
$f_{E,2}$ and σ_2 (km s^{-1})	$0.283^{+0.209}_{-0.092}$, 0.124
Derived quantities	
e	$0.51759^{+0.00076}_{-0.00081}$
ω_1 (deg)	$89.22^{+0.12}_{-0.11}$
i (deg)	$78.77^{+0.11}_{-0.11}$
M_1 ($M_\odot$)	$0.8252^{+0.0031}_{-0.0027}$
M_2 ($M_\odot$)	$0.7816^{+0.0027}_{-0.0022}$
$q \equiv M_2/M_1$	$0.9471^{+0.0017}_{-0.0019}$
a ($R_\odot$)	$25.733^{+0.030}_{-0.025}$
π_{orb} (mas)	$20.174^{+0.072}_{-0.072}$
Distance (pc)	$49.57^{+0.18}_{-0.18}$

Note. See Table 8 for the meaning of the error scale factors f, and rms residuals σ in the top portion of the table.

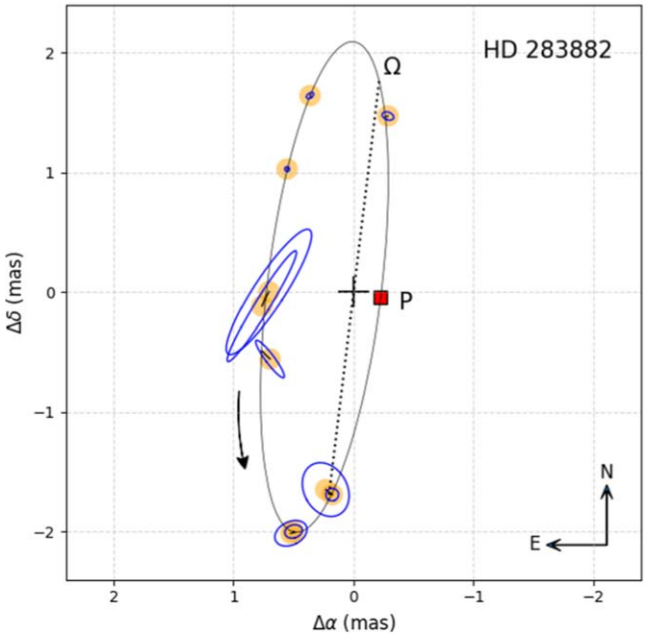

Figure 3. Astrometric measurements for HD 283882, as in Figure 1.

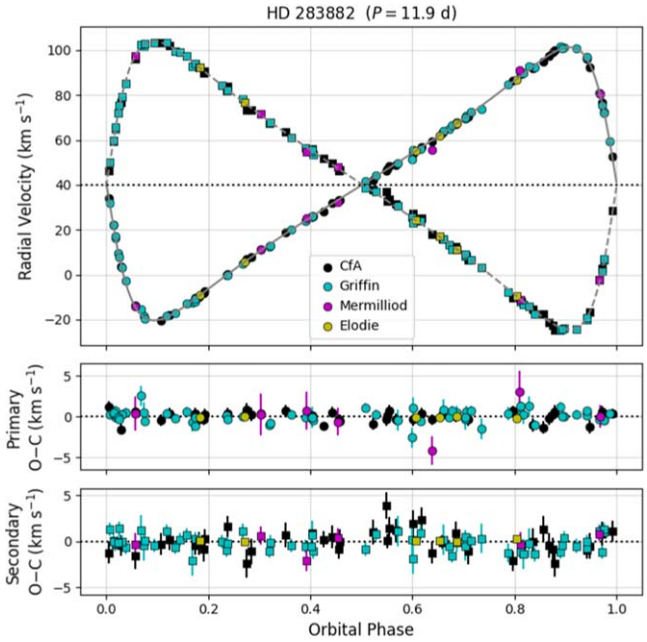

Figure 4. Same as Figure 2, for HD 283882.

between the Griffin, Mermilliod, and Elodie velocities and our own (Δ_G, Δ_M, Δ_E). The model and the observations are shown in Figures 3 and 4.

We note that the Gaia DR3 catalog reports a spurious spectroscopic orbital solution for HD 283882 (class "SB2") with a period of 82.8 days, velocity semiamplitudes of 83.4 and 79.9 km s^{-1} for the primary and secondary, and an eccentricity of 0.472. The period is not an integer multiple of the true period of 11.9 days. This appears to be an instance in which the fully automated Gaia procedures to solve for a spectroscopic orbit may have been fooled by the sparse coverage of the observations ($N = 14$), and/or possible confusion in the assignment of RVs to the primary or secondary, which are not very dissimilar in brightness. See also Bashi et al. (2022) and Rowan et al. (2023). It is possible that this problem will be resolved in future Gaia data releases, once additional observations are included.

HD 283882 is a well-known RS CVn object, and has been given the variable star designation V808 Tau. It is an X-ray source, and displays other typical signs of stellar activity, including emission cores in the Ca II H and K lines (Young 1974), Hα emission (Stauffer et al. 1991), and spot-induced brightness modulations (Bopp et al. 1980). The latter authors measured a peak-to-peak amplitude of 0.1 mag in the Strömgren b and y bands, and a rotation period of about 6.8 days, indicating nonsynchronous rotation. Similar rotational modulation is seen in the more recent photometry from TESS, along with frequent flares (see Section 7 below).

6.3. HD 26874

The binary nature of HD 26874 was announced by Griffin & Gunn (1981), who presented a double-lined spectroscopic orbit with a period of 55.1 days. Out of their 55 observations, about a dozen were taken at unfavorable phases with severe line blending, and were rejected by them. We retained 43 measurements for the primary and 41 for the secondary, made between 1974 and 1980, with relative weights as specified by the authors. We used their uncertainty of 0.8 km s^{-1} for an observation of unit weight in order to compute initial observational errors for our analysis. Griffin & Gunn (1981) pointed out that while HD 26874 lies above the color–magnitude diagram of the Hyades in combined light, when properly disentangled, the components fall slightly below it, suggesting the binary may lie on the far side of the cluster.

As was the case in the previous two systems, HD 26874 was observed with the CORAVEL instrument, and two RV measures made 4 days apart in 1979 were published by Mermilliod et al. (2009) for both components. In addition to these, our analysis incorporates seven observations (2003–2005) from the public Elodie archive, in which both components were measured. We assigned them arbitrary initial uncertainties of 0.5 km s^{-1}.

HD 26874 was monitored at the CfA with the digital speedometers between 1992 and 2004. The S/Ns of the 53 observations range from 10 to 33 per resolution element, the early ones being lower. The last visit used a longer exposure (S/N = 57). The templates adopted for the cross-correlations with TODCOR have temperatures of 5750 and 5250 K for the primary and secondary, and $v \sin i$ values of 4 and 6 km s^{-1}, respectively. The spectroscopic flux ratio is $(F_2/F_1)_{sp} = 0.508 \pm 0.018$.

The results of our MCMC analysis are given in Table 10, together with the systematic offsets we derived for the various RV data sets relative to ours, as well as the usual error inflation factors. Our orbital parallax for HD 26874 corresponds to a distance of 49 pc, which is in fact slightly behind the center of the cluster, as Griffin & Gunn (1981) suspected, by about 3.5 pc. Figure 5 illustrates the fit to the CHARA observations, and Figure 6 shows the RV observations.

The Washington Double Star Catalog (WDS; Worley & Douglass 1997; Mason et al. 2001) has an entry for HD 26874 as WDS J04157+2049A, and lists a common proper-motion companion some 145″ away, which is a faint and very red star (Reid 1992). In a subsequent paper, Reid & Gizis (1997) reported resolving this distant star with HST into two nearly equal components separated by 0.″88 (double star designation

Table 10
Results of Our Orbital Analysis for HD 26874

Parameter	Value
P (day)	$55.133176^{+0.000097}_{-0.000090}$
$T_{\rm peri}$ (HJD−2,400,000)	$50762.584^{+0.014}_{-0.015}$
a'' (mas)	$7.3382^{+0.0032}_{-0.0032}$
$\sqrt{e}\cos\omega_1$	$+0.22252^{+0.00054}_{-0.00059}$
$\sqrt{e}\sin\omega_1$	$+0.59340^{+0.00037}_{-0.00034}$
$\cos i$	$-0.66385^{+0.00040}_{-0.00037}$
Ω (deg)	$119.968^{+0.055}_{-0.051}$
γ (km s^{-1})	$+38.000^{+0.062}_{-0.062}$
K_1 (km s^{-1})	$27.498^{+0.038}_{-0.035}$
K_2 (km s^{-1})	$30.436^{+0.048}_{-0.048}$
$\Delta_{\rm G}$ (km s^{-1})	$-0.36^{+0.12}_{-0.12}$
$\Delta_{\rm M}$ (km s^{-1})	$-0.17^{+0.41}_{-0.27}$
$\Delta_{\rm E}$ (km s^{-1})	$+0.309^{+0.066}_{-0.066}$
$f_{\rm CHARA}$	$1.25^{+0.31}_{-0.19}$
$f_{\rm CfA,1}$ and σ_1 (km s^{-1})	$1.064^{+0.126}_{-0.099}$, 0.57
$f_{\rm CfA,2}$ and σ_2 (km s^{-1})	$0.770^{+0.090}_{-0.071}$, 0.62
$f_{\rm G,1}$ and σ_1 (km s^{-1})	$1.06^{+0.14}_{-0.10}$, 0.71
$f_{\rm G,2}$ and σ_2 (km s^{-1})	$1.01^{+0.13}_{-0.10}$, 1.30
$f_{\rm M,1}$ and σ_1 (km s^{-1})	$1.02^{+1.89}_{-0.50}$, 0.44
$f_{\rm M,2}$ and σ_2 (km s^{-1})	$0.62^{+1.04}_{-0.41}$, 0.25
$f_{\rm E,1}$ and σ_1 (km s^{-1})	$0.105^{+0.054}_{-0.025}$, 0.044
$f_{\rm E,2}$ and σ_2 (km s^{-1})	$0.159^{+0.071}_{-0.037}$, 0.069
Derived quantities	
e	$0.40164^{+0.00025}_{-0.00023}$
ω_1 (deg)	$69.444^{+0.060}_{-0.056}$
i (deg)	$131.594^{+0.029}_{-0.031}$
M_1 ($M_\odot$)	$1.0714^{+0.0040}_{-0.0036}$
M_2 ($M_\odot$)	$0.9682^{+0.0031}_{-0.0031}$
$q \equiv M_2/M_1$	$0.9035^{+0.0021}_{-0.0020}$
a ($R_\odot$)	$77.310^{+0.082}_{-0.082}$
$\pi_{\rm orb}$ (mas)	$20.411^{+0.026}_{-0.026}$
Distance (pc)	$48.994^{+0.063}_{-0.063}$

Note. See Table 8 for the meaning of the error scale factors f, and rms residuals σ in the top portion of the table.

RHy 119). Indeed, the Gaia DR3 catalog lists both of those red stars with a separation of 0.″86 in the N–S direction. They have G-band magnitudes of 16.0 and 16.1, more than 8 mag fainter than the primary ($G = 7.65$). These two faint objects have parallaxes and proper motions that identify them as members of the cluster, but that are somewhat different from those of HD 26874. In particular, the parallaxes are about 3 mas larger than that of the brighter star. At the distance to HD 26874, this corresponds to a linear separation of more than 6 pc along the line of sight, which is large enough to rule out association. On the other hand, the two fainter objects may well be orbiting each other, as their parallaxes are essentially the same, and their proper motions are quite similar.

6.4. HD 27149

The first indication that HD 27149 is a spectroscopic binary came from a report by Wilson (1948), who was not able to resolve the components. He only provided velocities from blended lines, which nevertheless showed significant variation. Woolley et al. (1960) were the first to successfully measure the

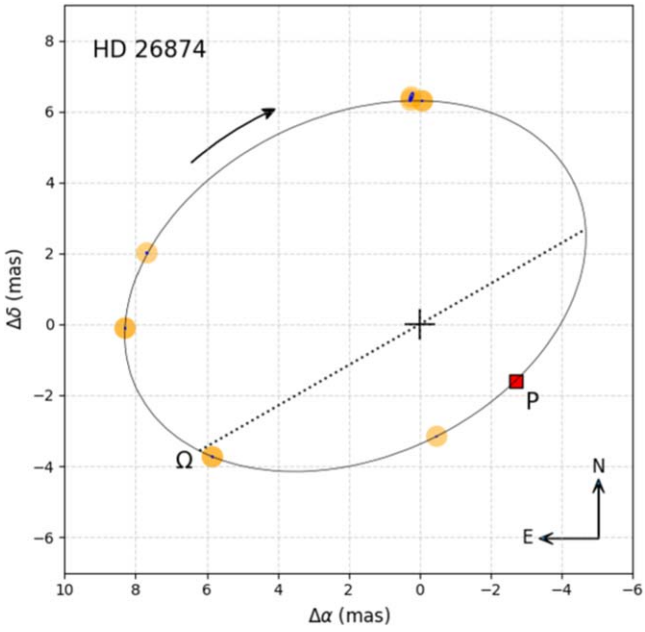

Figure 5. Astrometric measurements for HD 26874, as in Figure 1.

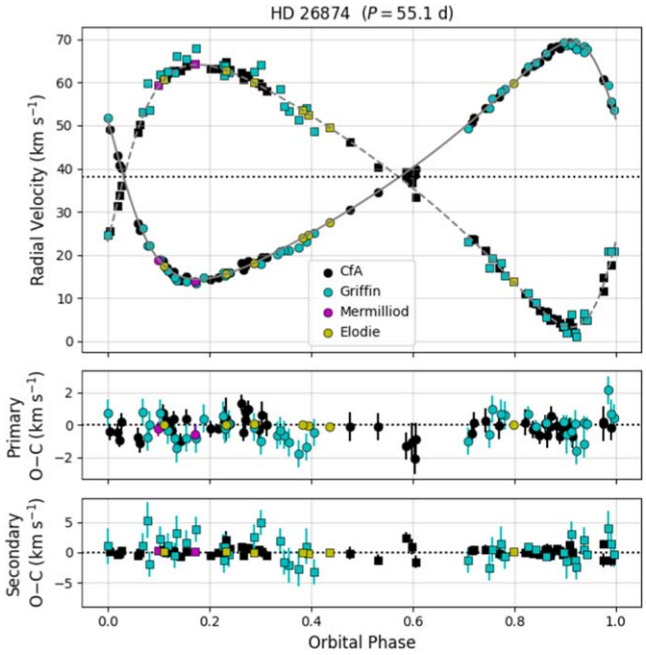

Figure 6. Same as Figure 2, for HD 26874.

primary and secondary separately. An orbital solution based on 34 measurements for both stars was later published by Batten & Wallerstein (1973), giving an orbital period of 75.6 days and a modest eccentricity of $e = 0.23$. Most of those observations were taken at relatively low dispersion, and are poor by today's standards. The eight higher dispersion measurements (4.5 and 6.5 Å mm^{-1}, from 1969–1971) are reasonably good, so we have chosen to use them here, assigning them an arbitrary initial uncertainty of 1 km s^{-1}. Five similar quality measurements from 1979 to 1981 were reported by McClure (1982), which we also incorporated into our modeling, adopting the same initial uncertainty of 1 km s^{-1}.

Additional velocities with much better precision were reported by Tomkin (2003), on the basis of which he significantly improved the spectroscopic orbital solution. We adopted his 1995–2002 measurements as published, with relative weights as given by the author and the standard error provided for an observation of unit weight (0.06 km s^{-1}). Three of the 50 epochs were excluded for having been made when the stars were near conjunction.

All but one of the 12 CORAVEL measurements from Mermilliod et al. (2009), gathered between 1978 and 1992, were incorporated into our analysis as well. The one excluded was taken when the lines were blended. A further seven pairs of RV measurements with the Elodie spectrograph (2003–2005) were obtained from the public archive, and were assumed initially to have the same uncertainty of 0.5 km s^{-1} assigned to them for other systems in this work.

HD 27149 was observed at the CfA between 1980 and 2001. We collected 71 usable spectra with the digital speedometers, at S/Ns of 11 to 35 per resolution element. We adopted templates with temperatures of 5750 and 5500 K for the primary and secondary, and rotational broadenings of 6 and 2 km s^{-1}. The primary value is consistent with independent measurements of 5.5 km s^{-1} by Strassmeier et al. (2000) and 7.1 ± 1.5 km s^{-1} by Mermilliod et al. (2009). We obtained an estimate of $(F_2/F_1)_{sp} = 0.610 \pm 0.015$ for the spectroscopic flux ratio at the mean wavelength of our observations.

This object was observed interferometrically in the K band with the PTI, between 2000 September and 2008 October. A total of 100 measurements of the squared visibilities were incorporated into our analysis. In addition to contributing to the orbital parameters, they allow an independent estimate of the flux ratio, $(F_2/F_1)_K$. Because the visibilities are invariant under a point-symmetric inversion around the binary origin, we restricted the flux ratio during the analysis to be smaller than unity, as expected for main-sequence stars with secondaries less massive than the primaries.

The parameters derived from our joint spectroscopic–astrometric solution are given in Table 11, with other derived properties at the bottom. See Figures 7 and 8 for graphical representations of the astrometric and RV observations, and the model. The PTI squared visibilities cannot be represented on the plane of the sky, but we show their phase coverage in Figure 7.

Batten & Wallerstein (1973) called attention to the large minimum masses for the components implied by their spectroscopic solution, which is about what one would expect from their spectral types. They mentioned the possibility of eclipses, a suggestion that has been repeated by many other authors since, and has prompted dedicated photometric efforts to search for those events (e.g., Jørgensen & Olsen 1972). See a detailed discussion of those observations by Tomkin (2003). Eclipses were never found, and our interferometric orbit from CHARA and the PTI now shows that the inclination angle (85°.9) is too low for that to occur. Eclipses would require it to be within about 1°.3 of edge-on (Tomkin 2003). The latter author noted that his greatly improved orbital solution provided the basis for an accurate orbital parallax for HD 27149, if only the pair could be resolved interferometrically, such as with the CHARA Array on Mt. Wilson that had just recently begun operations. With the present work, that promise is finally realized, some 20 yr later. The result is indeed very precise, with a formal parallax uncertainty of only 7.8 μas (0.04%), far better than Gaia DR3, which gives $\pi_{Gaia} = 21.606 \pm 0.042$ mas (including a zero-point correction following Lindegren et al. 2021b). The parallax values themselves do not agree.

As in the case of HD 283882, the Gaia DR3 catalog reports a spectroscopic orbit for HD 27149 (class "SB2C") that is erroneous: $P = 7.67$ days, $K_1 = 26.6$ km s^{-1}, $K_2 = 26.0$ km s^{-1}, and $e = 0$. This is another instance in which the automated orbit-solving algorithms seem to have failed. And once again, the number of RV measurements is small (only 13), and the components are relatively similar in brightness.

HD 27149 is also known as an RS CVn system (V1232 Tau). It was listed by Strassmeier et al. (2000) as having Ca II H and K emission, and brightness variations with a period of about 9

Table 11
Results of Our Orbital Analysis for HD 27149

Parameter	Value
P (day)	$75.658178^{+0.000062}_{-0.000062}$
T_{peri} (HJD−2,400,000)	$50160.429^{+0.012}_{-0.011}$
a'' (mas)	$9.6594^{+0.0023}_{-0.0023}$
$\sqrt{e}\cos\omega_1$	$-0.51993^{+0.00011}_{-0.00012}$
$\sqrt{e}\sin\omega_1$	$+0.01501^{+0.00067}_{-0.00057}$
$\cos i$	$-0.07204^{+0.00030}_{-0.00030}$
Ω (deg)	$133.169^{+0.015}_{-0.018}$
γ (km s^{-1})	$+38.927^{+0.065}_{-0.060}$
K_1 (km s^{-1})	$32.0741^{+0.0084}_{-0.0165}$
K_2 (km s^{-1})	$34.770^{+0.015}_{-0.015}$
$(F_2/F_1)_K$ from PTI	$0.763^{+0.086}_{-0.027}$
Δ_T (km s^{-1})	$+0.462^{+0.062}_{-0.060}$
Δ_M (km s^{-1})	$+0.27^{+0.18}_{-0.15}$
Δ_E (km s^{-1})	$+0.354^{+0.067}_{-0.062}$
Δ_{Mc} (km s^{-1})	$+0.14^{+0.35}_{-0.32}$
Δ_B (km s^{-1})	$+0.83^{+0.25}_{-0.32}$
f_{CHARA}	$1.14^{+0.36}_{-0.12}$
f_{PTI}	$1.086^{+0.095}_{-0.063}$
$f_{CfA,1}$ and σ_1 (km s^{-1})	$0.911^{+0.089}_{-0.070}$, 0.71
$f_{CfA,2}$ and σ_2 (km s^{-1})	$0.870^{+0.093}_{-0.057}$, 0.76
$f_{T,1}$ and σ_1 (km s^{-1})	$1.176^{+0.178}_{-0.091}$, 0.079
$f_{T,2}$ and σ_2 (km s^{-1})	$0.900^{+0.134}_{-0.068}$, 0.086
$f_{M,1}$ and σ_1 (km s^{-1})	$1.16^{+0.44}_{-0.14}$, 0.60
$f_{M,2}$ and σ_2 (km s^{-1})	$1.19^{+0.39}_{-0.17}$, 0.77
$f_{E,1}$ and σ_1 (km s^{-1})	$0.057^{+0.044}_{-0.010}$, 0.028
$f_{E,2}$ and σ_2 (km s^{-1})	$0.235^{+0.131}_{-0.041}$, 0.120
$f_{Mc,1}$ and σ_1 (km s^{-1})	$0.80^{+0.59}_{-0.11}$, 0.83
$f_{Mc,2}$ and σ_2 (km s^{-1})	$0.97^{+0.71}_{-0.13}$, 1.01
$f_{B,1}$ and σ_1 (km s^{-1})	$0.713^{+0.375}_{-0.083}$, 0.73
$f_{B,2}$ and σ_2 (km s^{-1})	$1.58^{+0.70}_{-0.24}$, 1.62
Derived quantities	
e	$0.26230^{+0.00012}_{-0.00010}$
ω_1 (deg)	$178.317^{+0.066}_{-0.072}$
i (deg)	$85.869^{+0.017}_{-0.017}$
M_1 ($M_\odot$)	$1.1028^{+0.0011}_{-0.0010}$
M_2 ($M_\odot$)	$1.01736^{+0.00072}_{-0.00109}$
$q \equiv M_2/M_1$	$0.92244^{+0.00044}_{-0.00062}$
a ($R_\odot$)	$96.706^{+0.028}_{-0.028}$
π_{orb} (mas)	$20.4783^{+0.0078}_{-0.0078}$
Distance (pc)	$46.559^{+0.017}_{-0.017}$

Note. See Table 8 for the meaning of the error scale factors f, and rms residuals σ in the top portion of the table.

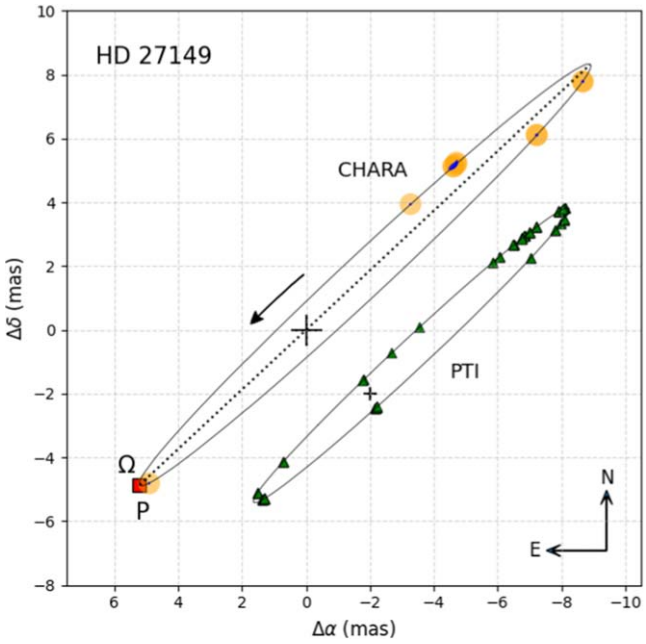

Figure 7. Astrometric measurements for HD 27149, as in Figure 1. The smaller ellipse is a scaled-down version of the orbit meant to show the location of the PTI squared visibility measurements (green triangles), which cannot be represented directly on the plane of the sky. Periastron passage happens to be very close to the ascending node in this nearly edge-on orbit.

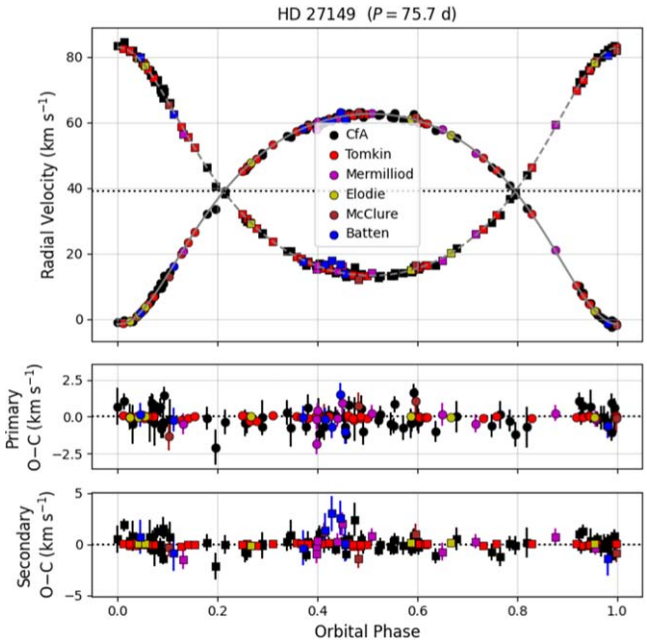

Figure 8. Same as Figure 2, for HD 27149.

days and an amplitude of 0.05 mag in the Strömgren *y* band. As shown later, the more recent TESS photometry shows a somewhat smaller photometric amplitude (∼0.028 mag) at the satellite's redder bandpass, and a similar though slightly longer period of 9.7 days. The object is also an X-ray source.

6.5. HD 30676

Early RV measurements for HD 30676 include three from 1961 by Woolley & Harding (1965), one from 1964 by Kraft (1965), and a few by other authors made at much lower dispersion, which have larger uncertainties. All of these are for the primary component only. While the first four are quite consistent with our orbit model below, we do not use them as they provide no significant improvement.

A spectroscopic orbit with a period of about 224.9 days was first reported by Mermilliod et al. (2009), from a series of 39 CORAVEL observations made between 1978 and 1991. Once again, only the primary was measured. Griffin (2012) published an additional 47 observations (1984–2007), in which he was able to measure the faint secondary component as well. In three of his observations, the stellar lines were blended, and those measures were rejected.

The CfA observations of HD 30676 consist of 27 spectra, gathered with the digital speedometer at the Oak Ridge Observatory in 1992–1997. The S/Ns range between about 10 and 41 per resolution element. The parameters of the primary template for the TODCOR analysis were set at $T_{\rm eff} = 6250$ K and $v \sin i = 12$ km s^{-1}. The secondary is too weak to determine those properties independently from our spectra with any confidence. We adopted best guesses of $T_{\rm eff} = 5000$ K and $v \sin i = 4$ km s^{-1}. The spectroscopic flux ratio is estimated to be $(F_2/F_1)_{\rm sp} = 0.060 \pm 0.012$.

Our MCMC solution used the CfA and CORAVEL RVs, as well as those of Griffin, with the relative weights he recommended. We initially adopted his uncertainty for an observation of unit weight of 0.39 km s^{-1}. As pointed out by Griffin (2012), the velocity measurements by Mermilliod et al. (2009), which were made without accounting for the presence of the secondary, are susceptible to "dragging" toward γ, particularly for the observations near conjunction. Griffin showed that an orbit for the primary, derived from those measurements alone, leads to a velocity semiamplitude slightly smaller than his to a statistically significant degree. Because of the desire to take advantage of the extended baseline afforded by the CORAVEL observations, Griffin first used them together with his own in a joint solution to improve the orbital period, and then carried out a final fit without them, but with the period held fixed at the previously determined value.

Here, we chose a different approach. Instead of fixing the period, which artificially suppresses correlations with other elements, we used the CORAVEL, Griffin, and CfA observations together to solve for all elements, but allowed the CORAVEL measurements for the primary to have their own velocity semiamplitude $K_{1,\rm COR}$, so as to not perturb the K_1 value from the others. The remaining elements were allowed to be shared. The results of this analysis are seen in Table 12. Our $K_{1,\rm COR}$ value is essentially the same as obtained by Griffin using the CORAVEL velocities alone (14.81 ± 0.16 km s^{-1}).

In view of our difficulty to determine the best TODCOR template for the faint secondary, and to guard against potential systematic errors in the RVs that may come from template mismatch, as a precaution, our analysis included one more free parameter, $\Delta_{\rm CfA}$, corresponding to an overall shift of our secondary velocities relative to those of the primary. The solution indicates this offset is not statistically significant. The astrometric measurements are displayed in Figure 9, and the RVs are seen in Figure 10.

The Gaia DR3 catalog reports an astrometric–spectroscopic orbital solution for HD 30676, of the kind referred to as "AstroSpectroSB1." Gaia does not resolve the pair, and can only measure the motion of the center of light. This time, the published orbit is correct, and the elements are very similar to

Table 12
Results of Our Orbital Analysis for HD 30676

Parameter	Value
P (day)	$224.9214^{+0.0038}_{-0.0039}$
$T_{\rm peri}$ (HJD−2,400,000)	$50512.61^{+0.13}_{-0.13}$
a'' (mas)	$21.4163^{+0.0084}_{-0.0084}$
$\sqrt{e}\cos\omega_1$	$-0.25776^{+0.00040}_{-0.00044}$
$\sqrt{e}\sin\omega_1$	$+0.31206^{+0.00056}_{-0.00056}$
$\cos i$	$-0.51238^{+0.00035}_{-0.00035}$
Ω (deg)	$320.142^{+0.043}_{-0.044}$
γ (km s^{-1})	$+41.310^{+0.081}_{-0.081}$
K_1 (km s^{-1})	$15.356^{+0.063}_{-0.064}$
K_2 (km s^{-1})	$23.58^{+0.34}_{-0.37}$
$K_{1,\rm COR}$ (km s^{-1})	$14.75^{+0.16}_{-0.17}$
$\Delta_{\rm G}$ (km s^{-1})	$-0.98^{+0.10}_{-0.10}$
$\Delta_{\rm M}$ (km s^{-1})	$-0.17^{+0.15}_{-0.15}$
$\Delta_{\rm CfA}$ (km s^{-1})	$-0.59^{+0.63}_{-0.64}$
$f_{\rm CHARA}$	$1.56^{+0.37}_{-0.22}$
$f_{\rm CfA,1}$ and σ_1 (km s^{-1})	$1.01^{+0.17}_{-0.12}$, 0.39
$f_{\rm CfA,2}$ and σ_2 (km s^{-1})	$0.81^{+0.15}_{-0.10}$, 3.04
$f_{\rm G,1}$ and σ_1 (km s^{-1})	$1.05^{+0.13}_{-0.10}$, 0.40
$f_{\rm G,2}$ and σ_2 (km s^{-1})	$1.46^{+0.18}_{-0.13}$, 1.95
$f_{\rm M,1}$ and σ_1 (km s^{-1})	$1.39^{+0.20}_{-0.14}$, 0.71
Derived quantities	
e	$0.16383^{+0.00022}_{-0.00022}$
ω_1 (deg)	$129.558^{+0.091}_{-0.091}$
i (deg)	$120.822^{+0.023}_{-0.023}$
M_1 ($M_\odot$)	$1.262^{+0.042}_{-0.042}$
M_2 ($M_\odot$)	$0.822^{+0.016}_{-0.016}$
$q \equiv M_2/M_1$	$0.6513^{+0.0107}_{-0.0098}$
a ($R_\odot$)	$198.9^{+1.8}_{-1.9}$
$\pi_{\rm orb}$ (mas)	$23.16^{+0.22}_{-0.21}$
Distance (pc)	$43.18^{+0.38}_{-0.42}$
ΔG (mag)	$2.420^{+0.049}_{-0.049}$
ΔHp (mag)	$2.39^{+0.92}_{-0.43}$

Note. See Table 8 for the meaning of the error scale factors f, and rms residuals σ in the top portion of the table. In this analysis, we have allowed the CORAVEL measurements of Mermilliod et al. (2009) to constrain their own velocity semiamplitude for the primary, $K_{1,\rm COR}$, independent of the K_1 value from the CfA and Griffin (2012) observations (see the text).

ours, although less precise. We reproduce them in Table 13 to facilitate the comparison. The main difference is a somewhat smaller eccentricity.

The combination of the semimajor axis of the photocenter from Gaia and the true relative semimajor axis from CHARA allows us to infer the brightness difference between the components at the Gaia wavelengths. This follows from the relation $a''_{\rm phot} = a''(B - \beta)$, where B is the secondary's fractional mass, and β is its fractional brightness. The fractional mass $B = M_2/(M_1 + M_2)$ is expressed in terms of the orbital elements as $B = K_1/(K_1 + K_2)$, and $\beta = (1 + 10^{0.4\Delta G})^{-1}$, where ΔG is the magnitude difference. We obtained $\Delta G = 2.420 \pm 0.049$ mag.

The Hipparcos catalog (Perryman et al. 1997; van Leeuwen 2007) did not include any information about the orbit, but did report an acceleration solution for HD 30676, i.e., one that required the derivatives of the proper-motion components, in addition to the five standard astrometric parameters, in order to properly model the motion on the plane of the sky. A test in which we used the intermediate astrometric data from the Hipparcos mission (abscissa residuals), together with all other observations, revealed that the satellite was quite capable of detecting the orbital motion of the photocenter. We obtained a semimajor axis very similar to that of Gaia ($a''_{\rm phot} = 6.34 \pm 1.03$). However, the much larger uncertainty makes the correspondingly uncertain inferred magnitude difference, $\Delta Hp = 2.39 \pm 0.92$ mag, too poor to be of much use.

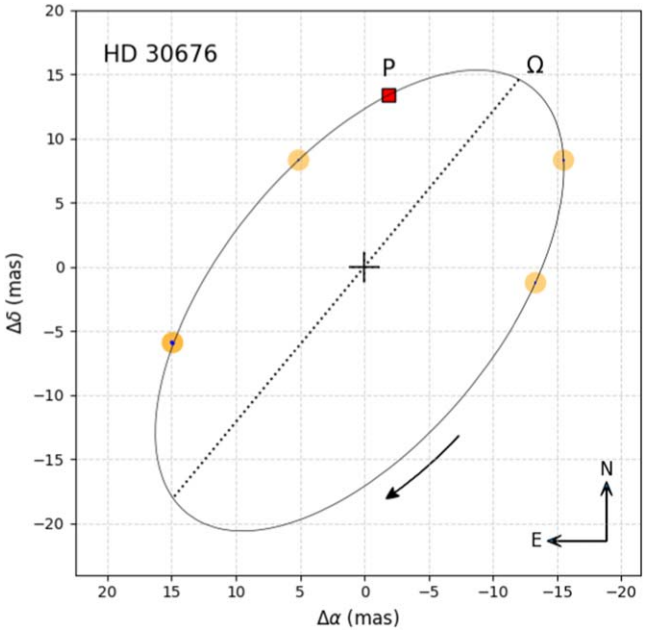

Figure 9. Astrometric measurements for HD 30676, as in Figure 1.

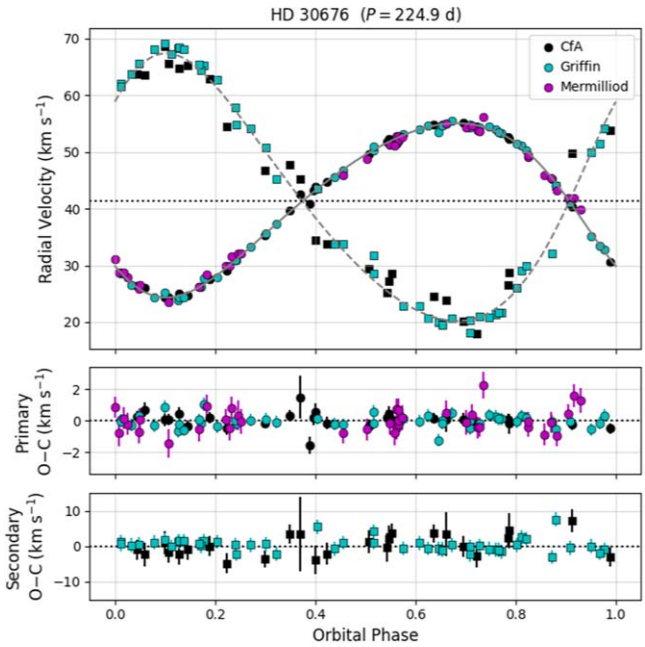

Figure 10. Same as Figure 2, for HD 30676.

6.6. HD 28545

The final object in our sample was first shown to be a spectroscopic binary by Griffin & Gunn (1981), based on

Table 13
Orbital Solution for HD 30676 from Gaia DR3

Parameter	Value
P (day)	224.78 ± 0.14
$T_{\rm peri}$ (HJD−2,400,000)[a]	57360.5 ± 1.1
$a''_{\rm phot}$ (mas)	6.366 ± 0.027
e	0.1465 ± 0.0039
ω_1 (deg)[b]	131.8 ± 1.8
i (deg)	120.63 ± 0.31
Ω (deg)[b]	320.45 ± 0.39
$\pi_{\rm Gaia}$ (mas)[c]	23.220 ± 0.023
γ (km s^{-1})	$+41.384 \pm 0.053$

Notes.
[a] Shifting this value backward by exactly 26 cycles using our more precise period yields $T_{\rm peri} = 2{,}451{,}512.8 \pm 1.1$, in good agreement with our value from Table 12.
[b] We have changed this angle by 180° because Gaia measured the photocenter, which is on the opposite side as the secondary relative to the center of mass.
[c] This is the Gaia parallax after accounting for orbital motion. Addition of the zero-point adjustment advocated by Lindegren et al. (2021b) results in the corrected value $\pi_{\rm Gaia} = 23.256 \pm 0.023$ mas.

observations taken at two different telescopes. The secondary was not detected. Their 46 measurements for the primary star were made between 1972 and 1980, two of which were rejected for giving large velocity residuals. Their orbit featured a modest eccentricity and a period of 358.4 days, which is so close to a year that a significant gap in their phase coverage was unavoidable. The only previous observations in the literature seem to be two measurements by Wilson (1948), which did not reveal the duplicity of the object.

HD 28545 was reobserved at the McDonald Observatory in 1995–2005 by Tomkin (2007), who detected and measured the weak secondary for the first time. He combined his observations with those of Griffin to produce an orbital solution with better phase coverage. In the process, he determined the offsets required for each of Griffin's two data sets in order to place them on the same velocity system as his. We adopted those offsets here as recommended by Tomkin (2007). We also used the relative weights for his observations, and for those of Griffin & Gunn (1981) established by Tomkin in that same combined solution, along with the corresponding 0.058 km s^{-1} error for an observation of unit weight that he reported. A total of 5 of the 33 Tomkin observations were affected by blending, and were excluded.

The velocity of HD 28545 was monitored at the CfA with the digital speedometers from 1979 to 2005. We gathered 75 observations with S/Ns between 9 and 57 per resolution element. Four additional spectra were obtained with TRES in 2011 and 2012, having S/Ns ranging from 50 to 131. The primary template for the cross-correlations with TODCOR used $T_{\rm eff} = 5250$ K and $v \sin i = 4$ km s^{-1}. As in the case of HD 30676, we were not able to establish the template parameters for the faint secondary independently. Our adopted template parameters for that star were 4500 K and 2 km s^{-1}. To account for possible biases in our secondary velocities that may come from template mismatch, our analysis allowed for a systematic offset relative to the RVs of the primary ($\Delta_{\rm CfA}$), although in the end the offset was insignificant. Our estimate of the flux ratio from our spectra is $(F_2/F_1)_{\rm sp} = 0.048 \pm 0.009$.

The Griffin & Gunn (1981) velocities precede both ours and those of Tomkin (2007), and are therefore useful for constraining

Table 14
Results of Our Orbital Analysis for HD 28545

Parameter	Value
P (day)	$358.4369^{+0.0060}_{-0.0060}$
$T_{\rm peri}$ (HJD−2,400,000)	$49268.91^{+0.15}_{-0.15}$
a'' (mas)	$23.745^{+0.024}_{-0.024}$
$\sqrt{e}\cos\omega_1$	$-0.4741^{+0.0014}_{-0.0014}$
$\sqrt{e}\sin\omega_1$	$+0.3821^{+0.0023}_{-0.0023}$
$\cos i$	$-0.4607^{+0.0014}_{-0.0014}$
Ω (deg)	$159.769^{+0.062}_{-0.063}$
γ (km s^{-1})	$+40.531^{+0.046}_{-0.042}$
K_1 (km s^{-1})	$14.028^{+0.022}_{-0.023}$
K_2 (km s^{-1})	$19.872^{+0.049}_{-0.049}$
$K_{1,\rm G}$ (km s^{-1})	$13.81^{+0.18}_{-0.18}$
$\Delta_{\rm CfA}$ (km s^{-1})	$+0.11^{+0.32}_{-0.32}$
$\Delta_{\rm T}$ (km s^{-1})	$-0.307^{+0.048}_{-0.045}$
$f_{\rm CHARA}$	$0.93^{+0.30}_{-0.16}$
$f_{\rm TRES,1}$ and σ_1 (km s^{-1})	$1.21^{+0.86}_{-0.36}$, 0.39
$f_{\rm TRES,2}$ and σ_2 (km s^{-1})	$3.17^{+1.96}_{-0.83}$, 2.64
$f_{\rm DS,1}$ and σ_1 (km s^{-1})	$0.764^{+0.073}_{-0.057}$, 0.12
$f_{\rm DS,2}$ and σ_2 (km s^{-1})	$0.564^{+0.055}_{-0.042}$, 3.22
$f_{\rm T,1}$ and σ_1 (km s^{-1})	$1.07^{+0.19}_{-0.13}$, 0.066
$f_{\rm T,2}$ and σ_2 (km s^{-1})	$0.94^{+0.16}_{-0.12}$, 0.190
$f_{\rm G,1}$ and σ_1 (km s^{-1})	$1.13^{+0.15}_{-0.11}$, 0.85
Derived quantities	
e	$0.3708^{+0.0013}_{-0.0013}$
ω_1 (deg)	$141.13^{+0.24}_{-0.24}$
i (deg)	$117.431^{+0.090}_{-0.091}$
M_1 ($M_\odot$)	$0.9717^{+0.0055}_{-0.0056}$
M_2 ($M_\odot$)	$0.6859^{+0.0028}_{-0.0028}$
$q \equiv M_2/M_1$	$0.7059^{+0.0022}_{-0.0022}$
a ($R_\odot$)	$251.30^{+0.41}_{-0.41}$
$\pi_{\rm orb}$ (mas)	$20.318^{+0.042}_{-0.042}$
Distance (pc)	$49.22^{+0.10}_{-0.10}$
ΔG (mag)	$2.016^{+0.041}_{-0.038}$

Note. See Table 8 for the meaning of the error scale factors f, and rms residuals σ in the top portion of the table. In this analysis, we have allowed the measurements of Griffin & Gunn (1981) to constrain their own velocity semiamplitude for the primary, $K_{1,\rm G}$, independent of the K_1 value from the CfA and Tomkin (2007) observations (see the text). $\Delta_{\rm CfA}$ is a velocity offset to be added to the secondary velocities from CfA to refer them to the same system as the primary velocities.

the orbital period. However, because they did not account for the presence of the unseen secondary, they could be biased toward γ and may affect the semiamplitude K_1 to some degree. As done in the previous section, our analysis allowed those velocities to contribute to all of the spectroscopic elements except for the semiamplitude, and a separate $K_{1,\rm G}$ value was added as a free parameter. Table 14 shows that the result for this additional parameter, $K_{1,\rm G} = 13.81 \pm 0.18$ km s^{-1}, is identical to that of Griffin & Gunn (1981). The difference compared to the K_1 value from the double-lined observations (14.028 ± 0.023 km s^{-1}) goes in the direction expected for a bias, but is only marginally significant.

Two CORAVEL observations from 1982 by Mermilliod et al. (2009) are hardly worth including, as they are only for the primary and may also be affected by blending. Figure 11 shows

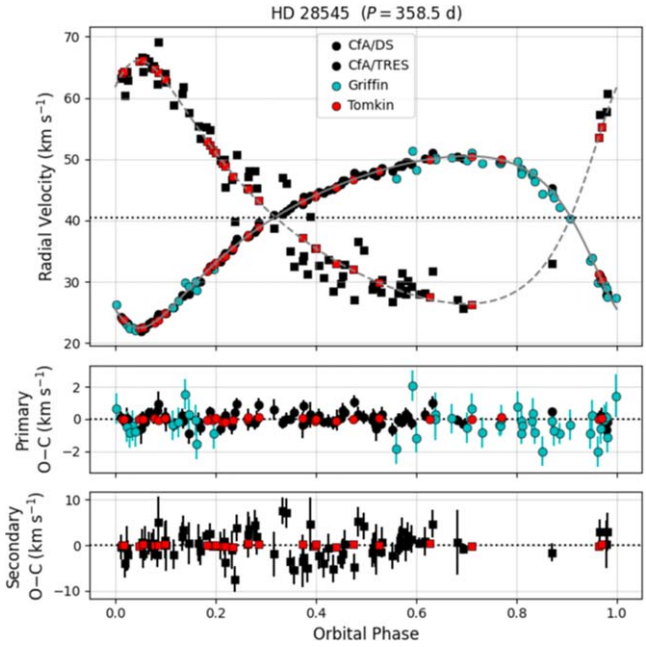

Figure 11. Same as Figure 2, for HD 28545.

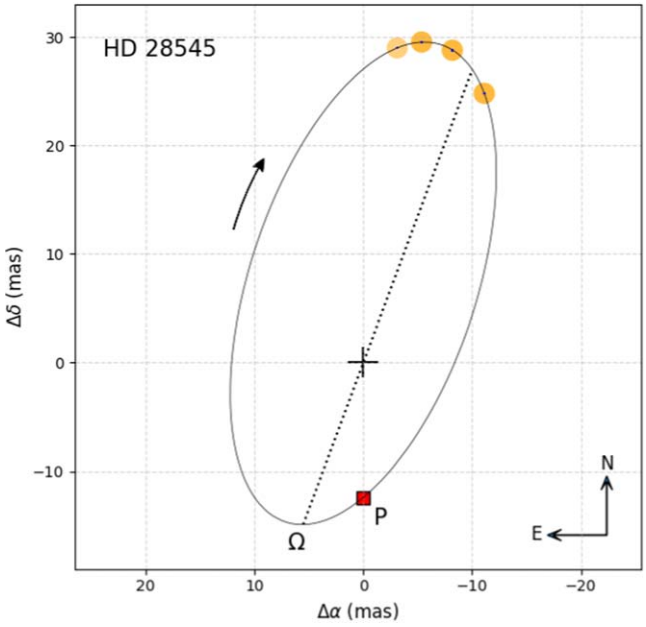

Figure 12. Astrometric measurements for HD 28545, as in Figure 1. See the text.

a plot of the RV observations used for the analysis, along with the model.

The CHARA measurements are shown graphically in Figure 12. They are seen to all be at one end of the orbit, which is a consequence of the seasonality of the scheduling at CHARA and the orbital period being so close to a year ($P = 358.4$ days). However, despite the poor phase coverage, most of the orbital elements are well determined by the spectroscopy, so the only astrometric elements that rely solely on the CHARA measurements (a'', i, Ω) are still reasonably well constrained by virtue of the very high precision achieved with the MIRC-X and MYSTIC beam combiners (typical separation errors of $\sim$10 μas). A small bias due to the incomplete phase coverage cannot be excluded, however, and additional measurements will be required to remove any doubt.

Table 15
Orbital Solution for HD 28545 from Gaia DR3

Parameter	Value
P (day)	357.95 ± 0.58
$T_{\rm peri}$ (HJD−2,400,000)[a]	57510.9 ± 1.7
$a''_{\rm phot}$ (mas)	6.62 ± 0.10
e	0.273 ± 0.025
ω_1 (deg)[b]	139.7 ± 2.4
i (deg)	118.1 ± 2.7
Ω (deg)[b]	160.0 ± 1.3
$\pi_{\rm Gaia}$ (mas)[c]	20.45 ± 0.26

Notes.
[a] Shifting this value backward by exactly 23 cycles using our more precise period yields $T_{\rm peri} = 2{,}449, 266.9 \pm 1.7$, in fair agreement with our value from Table 14.
[b] These angles, as reported by Gaia, are not correct for the photocenter. They are flipped by 180° (which is why they agree with ours), probably because there are no Gaia velocities with which to establish the correct quadrant.
[c] This is the Gaia parallax after accounting for orbital motion. Addition of the zero-point adjustment advocated by Lindegren et al. (2021b) results in the corrected value $\pi_{\rm Gaia} = 20.48 \pm 0.26$ mas.

A purely astrometric orbit for HD 28545 has been obtained by the Gaia mission, and reported as type "Orbital" in the DR3 catalog. Once again, the binary was not resolved, and the orbit corresponds to the photocenter. The elements are essentially correct, but have larger uncertainties than ours (see Table 15). The main difference is a smaller eccentricity, as was also the case for HD 30676. As in that system, we used the photocentric semimajor axis and relative semimajor axis to infer the brightness difference between the components of HD 28545 in the Gaia bandpass. We obtained $\Delta G = 2.016 \pm 0.041$ mag.

Our TRES spectra show the Ca II H and K lines in emission, indicating the system is chromospherically active. Additional comments on the activity are presented next.

7. Stellar Activity

All of our targets have been detected as X-ray sources (Voges et al. 1999, 2000), which is a sign of chromospheric activity. The X-ray luminosities (in ergs per second) range from $\log L_{\rm X} = 29.12$ to 29.64, except for HD 28545, which is weaker (28.45). Not surprisingly, they all also display photometric variability, as shown by the observations from TESS. Figure 13 collects the light curves from the satellite measured at a 2 minute cadence (simple aperture photometry), which we downloaded from the Mikulski Archive for Space Telescopes.[13] For display purposes, we have normalized the fluxes by dividing by the median in each of the observing sectors, ignoring any long-term trends. The total amplitudes over the entire observing period range from less than 5 mmag (HD 27483) to 55 mmag (HD 283882).

Under the common assumption that the variability is caused by spots carried around as the stars rotate, we have estimated the rotation periods from the average interval between maxima or minima. They are listed in Table 16, along with the peak-to-peak amplitudes. The two objects with the largest amplitudes,

[13] https://archive.stsci.edu

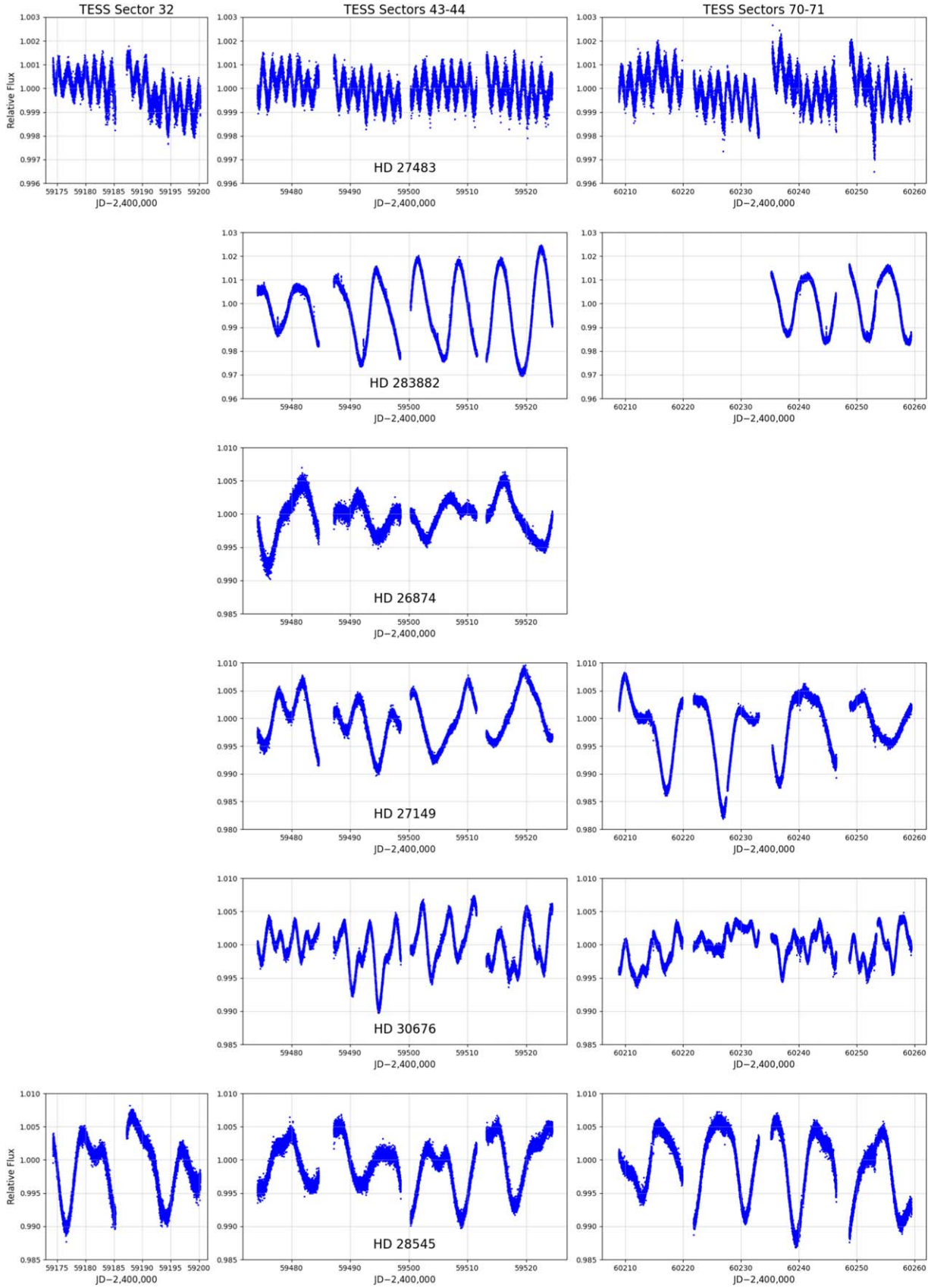

Figure 13. TESS light curves (at 2 minute cadence) for our six targets, one per row. Note that the vertical scales are different.

HD 283882 and HD 27149, have previously been recognized as RS CVn systems. In several cases, the complicated pattern of variation may constitute evidence that both components of the binary are spotted, or that one or both have more than one active region, or that the active regions evolve with time. Here, we have focused only on the dominant features in the light

Table 16
Estimated Rotation Periods of Our Targets from the TESS Photometry

Star	$P_{\rm rot}$ (day)	Total amplitude (mmag)
HD 27483	1.536 ± 0.012[a]	4.5
HD 283882	6.942 ± 0.050	55
HD 26874	8.54 ± 0.48	16
HD 27149	9.665 ± 0.086	28
HD 30676	4.361 ± 0.048	17
HD 28545	8.80 ± 0.10	20

Note.
[a] This is exactly half of the orbital period. Rather than rotation, this is most likely the period of the ellipsoidal variation (see the text).

curve, presumably due to the brighter primaries, and derived a single period.

Within the uncertainty, the period we derive for HD 27483 is exactly half of the orbital period. The light-curve maxima occur consistently at the orbital quadratures, and the minima at conjunctions. Given the short period of the binary ($P_{\rm orb} = 3.06$ days), the circular orbit, and the expectation that the stars' rotations should be synchronized with the orbital motion at the age of the Hyades, it seems likely that the photometric changes are caused in whole or at least in part by the reflection effect (ellipsoidal variation), which has a period of $P_{\rm orb}/2$. While spots cannot be entirely ruled out, they are less common in mid-F stars such as these.

HD 283882 has an orbital period long enough ($P_{\rm orb} =$ 11.93 days) that spin–orbit synchronization is not expected. However, its orbit happens to be the most eccentric in our sample ($e = 0.518$), and pseudosynchronization (Hut 1981) would lead to a rotation period near 4 days. The value we measure, which is closer to 7 days, would indicate it has not yet reached that state.

HD 283882 is also the only object in which we detect flares in the TESS light curves. A few of the more obvious ones are shown in Figure 14. By visual inspection, we detect approximately 30 of these events over a total time of observation of about 68 days, not counting gaps. The corresponding average flaring rate is about 0.44 flares per day, although this is likely to be a lower limit as we have only recorded ones that stand out clearly. Occasionally, these outbursts can occur much more frequently, as seen in two pairs of events in Figure 14 separated by just 1 or 2 hr. It is quite possible that both components are flaring (spectral types late G or early K).

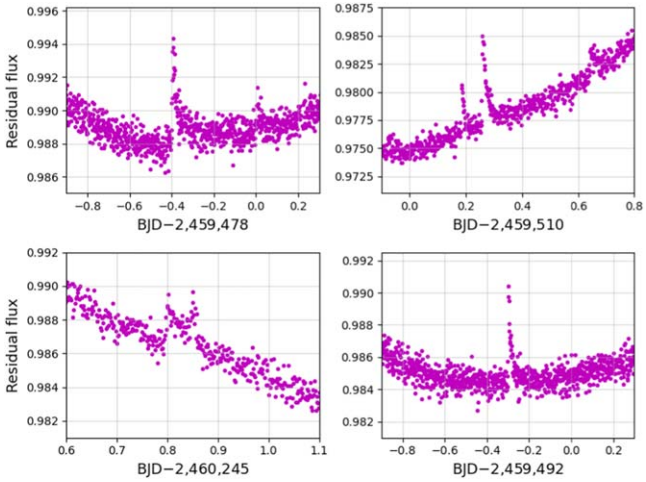

Figure 14. Examples of flares detected in the TESS light curve of HD 283882.

8. Discussion

For five of our six targets, we have determined the component masses with relative uncertainties in the range 0.1%–0.7%. The exception is HD 30676, which has errors of 3.3% and 1.9% for the primary and secondary, respectively, limited by the spectroscopy. Of all the previously published dynamical mass determinations in the Hyades, the only ones with formal errors of about 1% or better are for the eclipsing system HD 27130 (commonly known also as vB 22; Torres et al. 2002; Brogaard et al. 2021), and HD 284163, which is also part of our CHARA program and was reported separately (Torres et al. 2024a). We take this opportunity to collect in Table 17 all dynamical mass determinations for the main-sequence components of noninteracting binaries in the Hyades of which we are aware, published prior to this work. They span most of the main sequence in the cluster, from the A7 primary of θ^2 Tau to the early to mid M dwarfs in vA 351 BC.[14]

Most earlier mass determinations in the Hyades have been compared against stellar evolution models in a diagram of absolute V magnitude versus mass (see, e.g., Torres et al. 2019, and references therein). The spectroscopic flux ratios reported in this work allow us to add six more systems to that diagram, and our CHARA observations now enable a comparison in the near-infrared as well (H, K).

The flux ratios from our spectra correspond strictly to wavelengths centered on the region of the Mg I b triplet (~5187 Å). We have converted them to the more standard V band, by employing PHOENIX model spectra from Husser et al. (2013) to interpolate the flux ratios between 5187 Å and the H band, using appropriate temperatures for the binary components. We list these V-band ratios in Table 18, along with those in H and K from CHARA, averaged over all observations for each binary. We note that, although it is less precise, the K-band flux ratio from the PTI for HD 27149 (Table 11) agrees perfectly with the result from CHARA. Also included in Table 18 are the apparent V magnitudes of each object, taken from the homogeneous catalog of Mermilliod (1991), and the H and K magnitudes from Two Micron All Sky Survey (2MASS; Cutri et al. 2003). We used these, together with the orbital parallaxes from this work, to compute absolute magnitudes. Extinction is negligible for the Hyades.

The formal uncertainties for the flux ratios of HD 283882 in all three bandpasses are significantly larger than for the other five targets. The same is true of the V, H, and K magnitudes for the combined light. This extra scatter is caused by the high level of activity of the system, mentioned earlier. The masses and absolute magnitudes for the individual binary components of our six targets are collected in Table 19.

Figure 15 shows the empirical mass–luminosity relation for the cluster in the visual band, and includes the 10 systems in Table 17 and the six new ones from this work. The measurements are compared against two model isochrones with the same age and metallicity for the Hyades (750 Myr, [Fe/H] = + 0.18; Brandt & Huang 2015; Dutra-Ferreira et al. 2016). These properties were adopted here for consistency with other

[14] The latter system was overlooked in a few of the previous discussions of the empirical mass–luminosity relation (Torres et al. 2024a, 2024b).

Table 17
Previously Published Dynamical Mass Determinations in the Hyades

System	M_1 ($M_\odot$)	M_2 ($M_\odot$)	M_3 ($M_\odot$)	Reference
vB 22	1.0245 ± 0.0024	0.7426 ± 0.0016	⋯	Brogaard et al. (2021)
51 Tau	1.76 ± 0.08	1.47 ± 0.12	⋯	Anguita-Aguero et al. (2022)
θ^1 Tau[a]	⋯	1.28 ± 0.13	⋯	Lebreton et al. (2001)
θ^2 Tau	2.15 ± 0.12	1.87 ± 0.11	⋯	Armstrong et al. (2006)
70 Tau	1.363 ± 0.073	1.253 ± 0.075	⋯	Torres et al. (1997b)
vB 80	$1.63^{+0.30}_{-0.13}$	$1.11^{+0.21}_{-0.14}$	⋯	Torres (2019)
HD 28363	$1.341^{+0.026}_{-0.024}$	1.210 ± 0.021	0.781 ± 0.014	Torres et al. (2019)
vA 351 BC[b]	0.43 ± 0.04	0.41 ± 0.04	⋯	Benedict et al. (2021)
HD 284163	0.784 ± 0.011	0.5245 ± 0.0047	0.59 ± 0.12	Torres et al. (2024a)
vB 120	1.065 ± 0.018	1.008 ± 0.016	⋯	Torres et al. (2024b)

Notes.
[a] The primary of θ^1 Tau is a giant.
[b] This is a hierarchical quadruple system (AD + BC). The masses listed here correspond to stars B and C in the nomenclature of Benedict et al. (2021). BC is a close M-dwarf binary with a period of 0.75 day. Star A ($0.53 \pm 0.10\ M_\odot$) is presumed to be orbited in turn by a white dwarf (star D) with a mass of $0.54\ M_\odot$, and the AD pair orbits BC with a period of about 2.7 yr. We omit star A from this table on the grounds that it may have interacted with star D in the past. We also do not list the K dwarf primary in V471 Tau, an eclipsing postcommon envelope system in the Hyades (see, e.g., Muirhead et al. 2022), because of the prior interaction with its white dwarf companion.

Table 18
Combined-light Photometry, Flux Ratios, and Orbital Parallaxes for Our Targets

Target	$\pi_{\rm orb}$ (mas)	V (mag)	H (mag)	K_S (mag)	$(F_2/F_1)_V$	$(F_2/F_1)_H$	$(F_2/F_1)_K$
HD 27483	21.174 ± 0.073	6.173 ± 0.017	5.155 ± 0.024	5.062 ± 0.018	0.87 ± 0.03	0.932 ± 0.002	0.930 ± 0.003
HD 283882	20.174 ± 0.072	9.555 ± 0.031	7.120 ± 0.038	6.956 ± 0.038	0.61 ± 0.04	0.783 ± 0.039	0.811 ± 0.097
HD 26874	20.411 ± 0.026	7.835 ± 0.005	6.257 ± 0.017	6.190 ± 0.017	0.55 ± 0.02	0.719 ± 0.024	0.698 ± 0.002
HD 27149	21.4783 ± 0.0078	7.528 ± 0.011	6.032 ± 0.016	5.950 ± 0.017	0.64 ± 0.02	0.742 ± 0.016	0.763 ± 0.009
HD 30676	23.16 ± 0.22	7.114 ± 0.005	5.725 ± 0.023	5.666 ± 0.020	0.0850 ± 0.0012	0.233 ± 0.009	0.249 ± 0.009
HD 28545	20.318 ± 0.042	8.938 ± 0.009	6.902 ± 0.021	6.817 ± 0.018	0.0795 ± 0.0010	0.306 ± 0.009	0.337 ± 0.025

Table 19
Masses and Individual Absolute Magnitudes for Our Targets

Target	M_1 ($M_\odot$)	M_2 ($M_\odot$)	M_{V_1} (mag)	M_{V_2} (mag)	M_{H_1} (mag)	M_{H_2} (mag)	M_{K_1} (mag)	M_{K_2} (mag)
HD 27483	1.363 ± 0.010	1.3323 ± 0.0099	3.482 ± 0.025	3.633 ± 0.027	2.499 ± 0.025	2.575 ± 0.025	2.405 ± 0.020	2.484 ± 0.020
HD 283882	0.8252 ± 0.0029	0.7816 ± 0.0025	6.596 ± 0.042	7.133 ± 0.055	4.272 ± 0.045	4.537 ± 0.049	4.125 ± 0.070	4.352 ± 0.084
HD 26874	1.0714 ± 0.0038	0.9682 ± 0.0031	4.860 ± 0.015	5.509 ± 0.026	3.395 ± 0.023	3.753 ± 0.027	3.314 ± 0.017	3.705 ± 0.017
HD 27149	1.1028 ± 0.0011	1.01736 ± 0.00091	4.725 ± 0.017	5.210 ± 0.023	3.295 ± 0.019	3.619 ± 0.021	3.226 ± 0.018	3.519 ± 0.019
HD 30676	1.262 ± 0.042	0.822 ± 0.016	4.026 ± 0.006	6.703 ± 0.015	2.776 ± 0.024	4.358 ± 0.041	2.731 ± 0.021	4.241 ± 0.037
HD 28545	0.9717 ± 0.0056	0.6859 ± 0.0028	5.560 ± 0.010	8.310 ± 0.016	3.731 ± 0.023	5.017 ± 0.033	3.672 ± 0.028	4.853 ± 0.064

recent studies reporting dynamical mass determinations in the Hyades (Torres et al. 2019, 2024a, 2024b; Torres 2019). Overall, the isochrones follow the observed trend quite well, and there is very little difference between the PARSEC v1.2S model of Chen et al. (2014) and the MIST model of Choi et al. (2016). The most significant difference between the curves is at the low-mass end. Here, the models from the PARSEC series include an ad hoc adjustment to the temperature–opacity relation below $T_{\rm eff} = 4730$ K ($\sim 0.7\ M_\odot$), which was introduced by the builders to better reproduce the measured radii for M dwarfs in eclipsing binaries. Chen et al. (2014) argued that this also improves the fits in the color–magnitude diagrams of clusters.

A closer look at the stars with the more precise mass measurements reveals that the models seem to overestimate their brightness by a small amount. A similar observation has been made previously by Torres et al. (2024b), for the vB 120 system. The inset in Figure 15 shows this more clearly. It plots the M_V deviations (observed minus predicted) from the PARSEC v1.2S isochrone, for all stars with relative mass errors σ_M/M smaller than 4%, which includes all six binary systems in this paper. Note that, because of the slope of the mass–luminosity relation, the deviation ΔM_V from the model for any given star is different at $M + \sigma_M$ than at $M - \sigma_M$, resulting in the diagonal error bars in the figure. The same type of

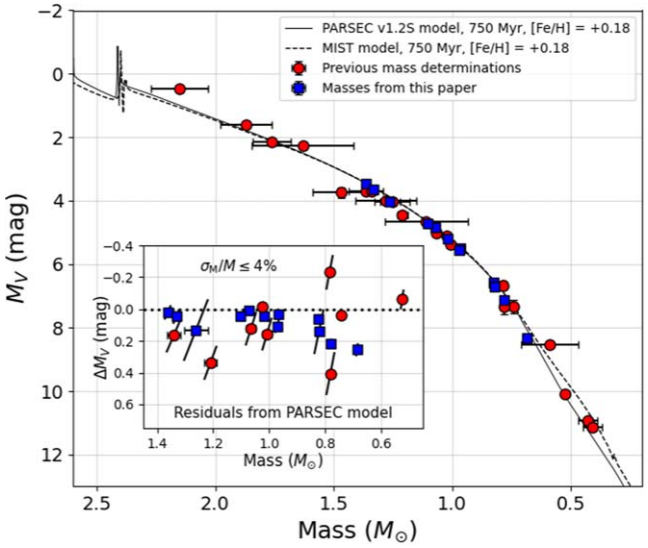

Figure 15. Empirical *V*-band mass–luminosity relation in the Hyades cluster, compared against two model isochrones, as labeled. The inset shows the difference in absolute magnitude from the PARSEC v1.2S model, restricted to stars with relative mass errors no larger than 4%. The differences in the sense observation minus model are predominantly positive, indicating theory overestimates the visual flux. Diagonal lines in the inset represent the deviation in the absolute magnitudes, factoring in the correlation with the mass errors (see the text).

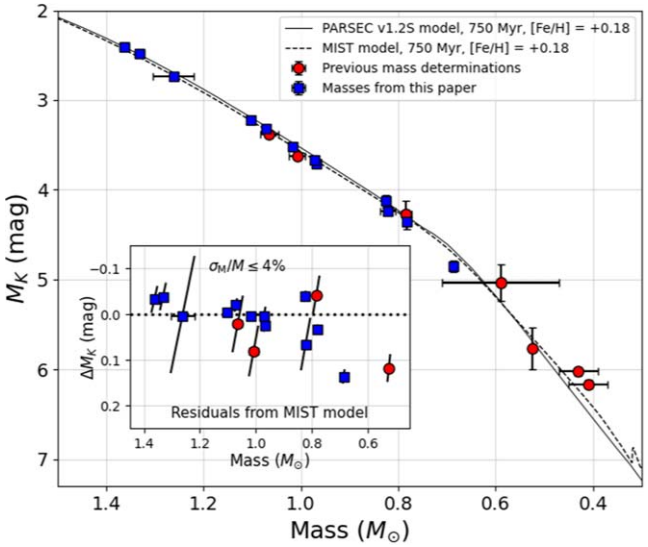

Figure 16. Similar to Figure 15, for the *K* band. In this case, the MIST model is a better fit to the observations.

comparison for the MIST model gives marginally larger deviations, in the same direction.

In principle, a different choice for the age and/or metallicity of the models could reduce the discrepancy with theory. The effect of those properties on the model predictions was discussed in detail by Torres et al. (2024b), who noted that age estimates for the Hyades have typically ranged between 625 and 800 Myr, and metallicity estimates range from about [Fe/H] = +0.1 to +0.2. The values adopted here are near the high end in both cases. Lowering the metallicity makes the models brighter, which would produce even larger differences between the models and the observations. Reducing the age, on the other hand, has a negligible effect on the brightness of stars of these masses because they are still unevolved at these ages. A systematic error in the observations themselves seems implausible, given that the various binary studies are largely independent. We conclude, therefore, that the deviations are real, and that, based on this sample of 21 stars between about 0.5 and 1.4 $M_\odot$, the PARSEC and MIST isochrones overestimate the visual flux by 0.096 ± 0.029 mag over this mass range, on average. A possible explanation is missing opacities in the models.

The situation changes toward the near-infrared. Figure 16 presents the empirical mass–luminosity in the (2MASS) *K* band, where fewer systems with dynamical masses and known component fluxes are available. At this wavelength, the MIST model is fainter than the PARSEC model by about 0.04 mag, and provides a better fit to the observations. The inset displays the brightness deviations from the MIST isochrone in the same way as before. The average ΔM_K difference from 16 stars (0.020 ± 0.013 mag) is now much smaller, and barely significant. The conclusion we draw is then that the MIST model is able to give a satisfactory match to the observations in *K*, at least over the mass range 0.5–1.4 $M_\odot$. The PARSEC model still overpredicts the *K*-band fluxes by a small amount, as noted above.

In the *H* band, we find a result that is intermediate between *V* and *K* (not shown). As above, the MIST isochrone is fainter than the one from PARSEC, and provides a better match to the observed fluxes, but still predicts the stars should be brighter. The average difference in M_H is 0.062 ± 0.017 mag, based on 14 stars over the same mass range as before.

A comparison between the orbital parallaxes of our six targets and those from Gaia is seen in Figure 17. For HD 30676 and HD 28545, the Gaia parallaxes we adopt are the ones corrected for orbital motion, as listed in Tables 13 and 15, respectively. In all cases except for one, our parallaxes and those from Gaia agree to within 2σ or better. The outlier is HD 27149, which happens to have the most precise orbital parallax in our sample ($\sigma_\pi = 7.8$ μas). The reasons for the large discrepancy are unclear, but may be related to the large RUWE value from Gaia for this object (RUWE = 1.936). Motion in the 75.6 day orbit was not accounted for in Gaia's astrometric solution, as it was for the longer-period binaries in our sample, and the much shorter spectroscopic period inferred by the mission is incorrect, as mentioned in Section 6.4. We estimate the amplitude (semimajor axis) of the motion of the photocenter of HD 27149 to be about 1.3 mas, and we speculate this could have affected the Gaia parallax.

Under the assumption that all Hyades members share a common space motion, the expected velocity of a star along the line of sight can be calculated from the cluster's space velocity vector and the sky position of the object. The predicted RVs for our six binary targets, based on the known space motion of the Hyades (Gaia Collaboration et al. 2018), are in good agreement with the measured center-of-mass velocities for five of them, with deviations $\gamma - RV_{\rm pred}$ ranging from -0.24 to $+0.57$ km s^{-1}. These differences are similar to, or just slightly larger than the velocity dispersion of the cluster adopted in the Gaia study mentioned above ($\sigma_{\rm cl} = 0.40$ km s^{-1}). The deviation for HD 27483, on the other hand, is about 2.5 times larger than $\sigma_{\rm cl}$ in absolute value, or -1.05 km s^{-1}. While an offset as large as this is not ruled out by statistics, we note that HD 27483 also happens to be the only target in our sample that is known to be in a triple system (see Section 6.1), and this could be affecting its measured γ velocity. Indeed, over the time interval covered by our observations, the expected RV of the binary in its ∼184 yr orbit around the white

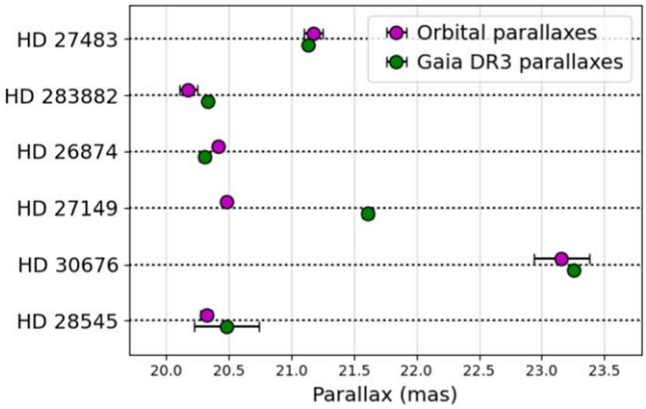

Figure 17. Comparison between the Gaia DR3 parallaxes (with the zero-point corrections of Lindegren et al. 2021b) and the orbital parallaxes determined in this work.

dwarf companion, based on the preliminary elements of Zhang et al. (2023), is about $-0.6\,\mathrm{km\,s^{-1}}$ from the center of mass of the triple. This accounts for a large fraction of the negative offset we find, bringing HD 27483 within a more comfortable 0.4 or $0.5\,\mathrm{km\,s^{-1}}$ of the expected velocity.

9. Conclusions

Using the CHARA Array, and in one case the PTI, we have spatially resolved six double-lined spectroscopic binaries in the Hyades. We have combined those observations with new and existing RV measurements, to derive high-precision dynamical masses for all components, in addition to the orbital parallaxes. When adding the determinations for HD 284163 reported separately (Torres et al. 2024a), our CHARA program has significantly increased the number of noninteracting systems with mass determinations in the cluster, from 9 to 16 (see Table 17).

Five of the six targets in this work have yielded masses with relative errors better than 1%, which are among the best in the Hyades to date. In one case (HD 27149), the uncertainty in our orbital parallax is only 7.8 μas (0.04%).

We have compared the properties of all systems with mass determinations in the cluster against predictions from two different models of stellar evolution (PARSEC v1.2S, and MIST). Isochrones calculated for an age and metallicity fixed to values appropriate for the Hyades follow the general trend in the empirical mass–luminosity relation relatively well in the V, H, and K bandpasses, over much of the main sequence. This test is valuable because it involves no free parameters in the comparison with the models. However, a closer look at the systems with the best mass measurements (0.5–1.4 $M_{\odot}$) reveals that model fluxes are slightly overestimated in the visual band over this range, by about 0.1 mag for the PARSEC isochrone. This may be due at least in part to missing opacities in the models. The deviation is marginally larger for MIST. We point out that it is unlikely that these disagreements can be eliminated with a different choice for the age and/or metallicity in the models, within reason. We find that the discrepancy is reduced toward the near-infrared: in the H band, it is about 0.06 mag for the MIST models, which perform better than PARSEC, and in the K band, the disagreement largely disappears for MIST, whereas a small difference remains for the PARSEC model.

All six of our targets display evidence of stellar activity, in the form of X-ray emission, and photometric variability caused by spots rotating in and out of view. We have estimated their rotation periods using the light curves from TESS. For HD 283882, we detected numerous flares, and estimate an average flaring rate of 0.44 events per day.

Acknowledgments

The spectroscopic observations at the CfA were obtained by P. Berlind, M. Calkins, J. Caruso, R. Davis, G. Esquerdo, J. Peters, E. Horine, and J. Zajac. We are grateful for their assistance.

We also thank R. J. Davis and J. Mink for maintaining the databases of echelle spectra, and the anonymous referee for a helpful suggestion. This work is based upon observations obtained with the Georgia State University Center for High Angular Resolution Astronomy Array at Mount Wilson Observatory. The CHARA array is supported by the National Science Foundation under grant Nos. AST-1636624 and AST-2034336. Institutional support has been provided from the GSU College of Arts and Sciences and the GSU Office of the Vice President for Research and Economic Development. MIRC-X received funding from the European Research Council (ERC) under the European Horizon 2020 research and innovation program (grant No. 639889). J.D.M. acknowledges funding for the development of MIRC-X (NASA-XRP NNX16AD43G, NSF-AST 1909165) and MYSTIC (NSF-ATI 1506540, NSF-AST 1909165). Time at the CHARA array was granted through the NOIRLab community access program (NOIRLab PropID: 2020B-0010, 2021B-0008, 2022B-235883; PI: G. Torres). This research has made use of the Jean-Marie Mariotti Center Aspro and SearchCal services. S.K. and C.L.D. acknowledge support by the European Research Council (ERC Starting grant, No. 639889 and ERC Consolidator grant, No. 101003096), and STFC Consolidated grant (ST/V000721/1). A.L. received funding from STFC studentship No. 630008203. The Palomar Testbed Interferometer was operated by the NASA Exoplanet Science Institute and the PTI collaboration. It was developed by the Jet Propulsion Laboratory, California Institute of Technology with funding provided from the National Aeronautics and Space Administration.

This research has benefited from the use of the SIMBAD and VizieR databases, operated at the CDS, Strasbourg, France, of NASA's Astrophysics Data System Abstract Service, and of the WEBDA database, operated at the Department of Theoretical Physics and Astrophysics of the Masaryk University (Czech Republic). The work has also made use of data from the European Space Agency (ESA) mission Gaia (https://www.cosmos.esa.int/gaia), processed by the Gaia Data Processing and Analysis Consortium (DPAC, https://www.cosmos.esa.int/web/gaia/dpac/consortium). Funding for the DPAC has been provided by national institutions, in particular the institutions participating in the Gaia Multilateral Agreement. The computational resources used for this research include the Smithsonian High Performance Cluster (SI/HPC), Smithsonian Institution (https://doi.org/10.25572/SIHPC).

ORCID iDs

Guillermo Torres https://orcid.org/0000-0002-5286-0251
Stefan Kraus https://orcid.org/0000-0001-6017-8773
Cyprien Lanthermann https://orcid.org/0000-0001-9745-5834
John D. Monnier https://orcid.org/0000-0002-3380-3307

References

Anguita-Aguero, J., Mendez, R. A., Clavería, R. M., et al. 2022, AJ, 163, 118
Anderson, J. A. 1920, ApJ, 51, 263
Anugu, N., Le Bouquin, J.-B., Monnier, J. D., et al. 2020, AJ, 160, 158
Armstrong, J. T., Mozurkewich, D., Hajian, A. R., et al. 2006, AJ, 131, 2643
Baines, E. K., Armstrong, J. T., Schmitt, H. R., et al. 2018, AJ, 155, 30
Barstow, M. A., Bond, H. E., Burleigh, M. R., et al. 2001, MNRAS, 322, 891
Bashi, D., Shahaf, S., Mazeh, T., et al. 2022, MNRAS, 517, 3888
Batten, A. H., & Wallerstein, G. 1973, PDAO, 14, 135
Benedict, G. F., Franz, O. G., Horch, E. P., et al. 2021, AJ, 161, 285
Boden, A. F., van Belle, G. T., Colavita, M. M., et al. 1998, ApJL, 504, L39
Böhm-Vitense, E. 1993, AJ, 106, 1113
Bopp, B. W., Noah, P. V., & Klimke, A. 1980, AJ, 85, 1386
Bourgés, L., Lafrasse, S., Mella, G., et al. 2014, in ASP Conf. Ser. 485, Astronomical Data Analysis Software and Systems XXIII, 485, ed. N. Manset & P. Forshay, 223
Boyajian, T. S., McAlister, H. A., Cantrell, J. R., et al. 2009, ApJ, 691, 1243
Brandt, T. D., & Huang, C. X. 2015, ApJ, 807, 58
Brogaard, K., Pakštienė, E., Grundahl, F., et al. 2021, A&A, 645, A25
Chen, Y., Girardi, L., Bressan, A., et al. 2014, MNRAS, 444, 2525
Choi, J., Dotter, A., Conroy, C., et al. 2016, ApJ, 823, 102
Christie, W. H., & Wilson, O. C. 1938, ApJ, 88, 34
Colavita, M., Akeson, R., Wizinowich, P., et al. 2003, ApJL, 592, L83
Colavita, M. M., Wallace, J. K., Hines, B. E., et al. 1999, ApJ, 510, 505
Cutri, R. M., Skrutskie, M. F., van Dyk, S., et al. 2003, The IRSA 2MASS All-Sky Point Source Catalog, NASA/IPAC Infrared Science Archive, http://irsa.ipac.caltech.edu/applications/Gator/
Dutra-Ferreira, L., Pasquini, L., Smiljanic, R., et al. 2016, A&A, 585, A75
Eisenhauer, F., Monnier, J. D., & Pfuhl, O. 2023, ARA&A, 61, 237
Fűrész, G. 2008, PhD thesis, Univ. Szeged, Hungary
Foreman-Mackey, D., Hogg, D. W., Lang, D., & Goodman, J. 2013, PASP, 125, 306
Gaia Collaboration, Babusiaux, C., van Leeuwen, F., et al. 2018, A&A, 616, A10
Gaia Collaboration, Vallenari, A., Brown, A. G. A., et al. 2023, A&A, 674, A1
Gelman, A., & Rubin, D. B. 1992, StaSc, 7, 457
Gregory, P. C. 2005, ApJ, 631, 1198
Griffin, R. F. 2012, JApA, 33, 29
Griffin, R. F., & Gunn, J. E. 1978, AJ, 83, 1114
Griffin, R. F., & Gunn, J. E. 1981, AJ, 86, 588
Husser, T.-O., Wende-von Berg, S., Dreizler, S., et al. 2013, A&A, 553, A6
Hut, P. 1981, A&A, 99, 126
Jørgensen, B. G., & Olsen, E. H. 1972, IBVS, 652, 1
Konacki, M., & Lane, B. F. 2004, ApJ, 610, 443
Kraft, R. P. 1965, ApJ, 142, 681
Latham, D. W. 1992, in ASP Conf. Ser. 32, IAU Coll. 135, Complementary Approaches to Double and Multiple Star Research, ed. H. A. McAlister & W. I. Hartkopf (San Francisco, CA: ASP), 110
Latham, D. W., Nordstroem, B., Andersen, J., et al. 1996, A&A, 314, 864
Latham, D. W., Stefanik, R. P., Torres, G., et al. 2002, AJ, 124, 1144
Lebreton, Y., Fernandes, J., & Lejeune, T. 2001, A&A, 374, 540
Lindegren, L. 2018, Gaia Data Processing & Analysis Consortium Publication GAIA-C3-TN-LU-LL-124-01, https://www.cosmos.esa.int/web/gaia/public-dpac-documents
Lindegren, L., Bastian, U., Biermann, M., et al. 2021b, A&A, 649, A4
Lindegren, L., Klioner, S. A., Hernández, J., et al. 2021a, A&A, 649, A2
Mason, B. D., Wycoff, G. L., Hartkopf, W. I., et al. 2001, AJ, 122, 3466
Mayor, M., & Mazeh, T. 1987, A&A, 171, 157
McClure, R. D. 1982, ApJ, 254, 606
Mermilliod, J. C. 1991, Catalogue of Homogeneous Means in the UBV System, Institut d'Astronomie, Universite de Lausanne, https://vizier.cds.unistra.fr/viz-bin/VizieR?-source=II/168
Mermilliod, J.-C., Mayor, M., & Udry, S. 2009, A&A, 498, 949
Merrill, P. W. 1922, ApJ, 56, 40
Monnier, J. D. 2003, RPPh, 66, 789
Monnier, J. D. 2007, NewAR, 51, 604
Morales, L. M., Sandquist, E. L., Schaefer, G. H., et al. 2022, AJ, 164, 34
Muirhead, P. S., Nordhaus, J., & Drout, M. R. 2022, AJ, 163, 34
Nordström, B., Latham, D. W., Morse, J. A., et al. 1994, A&A, 287, 338
Northcott, R. J., & Wright, K. O. 1952, JRASC, 46, 11
Perryman, M. A. C., Lindegren, L., Kovalevsky, J., et al. 1997, A&A, 323, L49
Quirrenbach, A. 2001a, ARA&A, 39, 353
Quirrenbach, A. 2001b, in IAU Symp. 200, The Formation of Binary Stars, ed. H. Zinnecker & R. D. Mathieu, 539
Reid, I. N., & Gizis, J. E. 1997, AJ, 114, 1992
Reid, N. 1992, MNRAS, 257, 257
Ricker, G. R., Winn, J. N., Vanderspek, R., et al. 2015, JATIS, 1, 014003
Rowan, D. M., Jayasinghe, T., Stanek, K. Z., et al. 2023, MNRAS, 523, 2641
Salsi, A., Nardetto, N., Mourard, D., et al. 2021, A&A, 652, 26
Schaefer, G. H., Hummel, C. A., Gies, D. R., et al. 2016, AJ, 152, 213
Setterholm, B., Monnier, J. D., Le Bouquin, J.-B., et al. 2023, JATIS, 9, 025006
Stauffer, J. R., Giampapa, M. S., Herbst, W., et al. 1991, ApJ, 374, 142
Stefanik, R. P., Latham, D. W., & Torres, G. 1999, in IAU Colloq. 170, Precise Stellar Radial Velocities, 185, ed. J. B. Hearnshaw & C. D. Scarfe (Cambridge: Cambridge Univ. Press), 354
Strassmeier, K., Washuettl, A., Granzer, T., et al. 2000, A&AS, 142, 275
Szentgyorgyi, A. H., & Fűrész, G. 2007, in 3rd Mexico-Korea Conference on Astrophysics: Telescopes of the Future and San Pedro Mártir, ed. S. Kurtz et al. (Mexico City: Universidad Nacional Autonoma de Mexico), 129
ten Brummelaar, T. A., McAlister, H. A., Ridgway, S. T., et al. 2005, ApJ, 628, 453
Tokovinin, A., Thomas, S., Sterzik, M., et al. 2006, A&A, 450, 681
Tomkin, J. 2003, Obs, 123, 1
Tomkin, J. 2007, Obs, 127, 165
Torres, G. 2019, ApJ, 883, 105
Torres, G., Andersen, J., & Giménez, A. 2010, A&ARv, 18, 67
Torres, G., Neuhäuser, R., & Guenther, E. W. 2002, AJ, 123, 1701
Torres, G., Schaefer, G. H., Stefanik, R. P., et al. 2024a, MNRAS, 527, 8907
Torres, G., Stefanik, R. P., Andersen, J., et al. 1997a, AJ, 114, 2764
Torres, G., Stefanik, R. P., & Latham, D. W. 1997b, ApJ, 479, 268
Torres, G., Stefanik, R. P., & Latham, D. W. 2019, ApJ, 885, 9
Torres, G., Stefanik, R. P., & Latham, D. W. 2024b, ApJ, 960, 121
van Leeuwen, F. 2007, A&A, 474, 653
Voges, W., Aschenbach, B., Boller, T., et al. 1999, A&A, 349, 389
Voges, W., Aschenbach, B., Boller, T., et al. 2000, IAU Circ., 7432, 3
Wallace, J. K., Boden, A. F., Colavita, M. M., et al. 1998, Proc. SPIE, 3350, 864
Wilson, R. E. 1948, ApJ, 107, 119
Woolley, R. R., Jones, D. H. P., & Mather, L. M. 1960, RGOB, 23, 1
Woolley, S. R., & Harding, G. A. 1965, RGOB, 93, 363
Worley, C. E., & Douglass, G. G. 1997, A&AS, 125, 523
Young, A. 1974, PASP, 86, 59
Young, R. K. 1939, PDDO, 1, 69
Zhang, H., Brandt, T. D., Kiman, R., et al. 2023, MNRAS, 524, 695
Zucker, S., & Mazeh, T. 1994, ApJ, 420, 806